A molecular mechanism by which amyloid-β induces transcriptional inactivation of CREB in Alzheimer's Disease

Katarzyna M. Grochowska[1,2*], Rahul Kaushik[1,3*], Guilherme M. Gomes[1,6*], Rajeev Raman[1*], Julia Bär[1], Gonca Bayraktar[1], Sebastian Samer[1], Irene Reyes-Resina[1], Christina Spilker[1], Markus Morawski[4], Steffen Rossner[4], Gemma Navarro Brugal[5], Anna Karpova[1,6#*], Michael R. Kreutz[1,2,3,6#]

[1]RG Neuroplasticity, Leibniz Institute for Neurobiology, Magdeburg, Germany
[2]Leibniz Group 'Dendritic Organelles and Synaptic Function', Center for Molecular Neurobiology (ZMNH), University Medical Center Hamburg-Eppendorf, Hamburg, Germany
[3]German Center for Neurodegenerative Diseases (DZNE), Magdeburg, Germany
[4]Molecular Imaging in Neurosciences, Paul Flechsig Institute of Brain Research, Leipzig, Germany
[5]Centro de Investigación Biomédica en Red Sobre Enfermedades Neurodegenerativas and Department of Biochemistry and Molecular Biology, Faculty of Biology, University of Barcelona, Barcelona, Spain
[6]Center for Behavioral Brain Sciences, Otto von Guericke University, Magdeburg, Germany

*Equal contribution
#Shared correspondence

Running title: Jacob induces CREB shut-off

The authors declare that they have no conflict of interest.

Abstract

Disruption of transcriptional activity of cAMP–responsive element-binding protein (CREB), a master regulator of cell survival and plasticity-related gene expression, is a hallmark of neurodegenerative diseases. CREB shut-off results in synaptic dysfunction and neuronal cell death and is elicited in Alzheimer's disease (AD) by amyloid-β-induced activation of extrasynaptic N-methyl-D-aspartate-receptors (NMDAR). Following long-distance transport from NMDAR to the nucleus the protein messenger Jacob docks a signalosome to CREB that encodes the synaptic or extrasynaptic origin of the NMDAR signal. In previous work we found that in response to cell survival/plasticity related synaptic NMDAR stimulation macromolecular transport of Jacob docks the MAP-kinase ERK to the CREB complex which results in sustained CREB phosphorylation. Here we show that in case of disease-related activation of extrasynaptic NMDAR by amyloid-β, Jacob associates with protein phosphatase-1γ (PP1γ) and induces dephosphorylation and transcriptional inactivation of CREB. Binding of the adaptor protein LIM domain only 4 (LMO4) to Jacob distinguishes extrasynaptic from synaptic NMDAR signaling and determines the affinity for the association with PP1γ. This mechanism contributes to transcriptional inactivation of CREB in response to extrasynaptic NMDAR signaling in the context of early synaptic dysfunction and cell loss in AD. Accordingly, Jacob protein knockdown attenuates CREB shut-off and cellular deterioration in response to amyloid-β signaling and Jacob gene knock out is neuroprotective in a transgenic mouse model of AD.

Keywords: NMDA-receptor, Alzheimer's disease, LMO4, CREB, cell death, Jacob, *Nsmf*, α-internexin, PP1γ

Introduction

NMDAR are heterotetrameric glutamate-gated ion channels that have been implicated in synaptic plasticity, learning, memory, and cell survival signaling but also in neurodegeneration and excitotoxicity (1-4). A prevailing hypothesis in the field suggests that the opposing functions of NMDAR can be attributed to their subunit composition and subcellular localization (1, 5, 6). In particular activation of GluN2B containing NMDAR at extrasynaptic sites has been implicated in brain disease states such as stroke, hypoxia, ischemia, Huntington's, and Alzheimer's disease (AD) and proved to be an interesting therapeutic target (1, 2, 5-11). Signaling downstream of synaptic and extrasynaptic NMDAR is tightly and antagonistically coupled to the activity of the transcription factor cAMP-responsive element-binding protein (CREB). Activation of synaptic NMDAR activates CREB through sustained phosphorylation of a crucial serine at position 133 and thereby promotes the expression of plasticity-related genes (2, 12, 13). Several studies have shown that gene expression programs that are triggered by CREB following activation of synaptic NMDAR are critically involved in learning and memory processes (14, 15). Conversely, predominant activation of extrasynaptic NMDAR leads to sustained dephosphorylation of CREB, also known as CREB shut-off, rendering CREB transcriptionally inactive (16). Loss of CREB dependent gene expression after extrasynaptic NMDAR activation is a major event preceding cell death and neurodegeneration (2, 17-20). Especially in AD, dysregulation of CREB dependent gene expression apparently plays a role in the onset of the disease and early synaptic dysfunction (18, 19, 21-26). The underlying mechanisms, as well as their relevance or contribution to Aβ-mediated CREB shut-off and neurodegeneration in AD, are still unknown (18, 19).

In previous work, we could show that the synapto-nuclear messenger Jacob, following long-distance transport and nuclear import, can encode and transduce the synaptic and extrasynaptic origin of GluN2B NMDAR signals to the nucleus (27-29). Activation of synaptic NMDARs leads to phosphorylation of Jacob at serine 180 via ERK1/2 kinase, which is followed by trafficking along microtubules of a pJacob/pERK1/2 signalosome to neuronal nuclei (27). Binding of the intermediate filament α-internexin at the N-terminus of Jacob protects pJacob and pERK against dephosphorylation during transport (28). By yet unknown mechanisms this signalosome promotes CREB phosphorylation at serine 133 and hence CREB dependent gene expression. On the contrary, activation of extrasynaptic NMDAR using

bath NMDA or exogenous Aβ application leads to prominent translocation of non-phosphorylated Jacob and induces CREB shut-off followed by stripping of synaptic contacts, simplification of dendritic arborization and cell death (30-32). Taken together the data indicate that Jacob operates as a mobile hub that docks NMDAR-derived signalosomes to nuclear target sites (27, 28). However, the molecular mechanisms behind the ambidextrous regulation of CREB by Jacob upon synaptic and extrasynaptic NMDAR stimulation are not yet clear. In the present study, we addressed two fundamental questions. We first investigated the coupling of extrasynaptic NMDAR signaling to CREB and deciphered the molecular mechanisms of Jacob-induced CREB shut-off. Next, we assessed the physiological significance of this mechanism for neurodegeneration in AD in transgenic mice and human brain tissue.

Results

Jacob is a direct binding partner of CREB

In previous work we have reported a functional association of Jacob with CREB (27, 28) but we have not established a direct interaction. To follow up on this and to decipher the molecular mechanism behind Jacob-induced CREB shut-off we first asked whether both proteins might be in one complex *in vivo*. Super-resolution stimulated emission depletion (STED) imaging revealed indeed a tight association of CREB with Jacob in the nucleus of cultured hippocampal neurons (Fig. 1A, B). We could also co-immunoprecipitate endogenous CREB from HEK293T cells following heterologous expression of Jacob (Fig. 1 C), indicating that the interaction is not depending on the cytomatrix of neuronal nuclei. A direct interaction was then confirmed by pull-down of bacterially expressed CREB and Jacob coupled to the matrix (Fig. 1D, Fig S1A). To map the minimal binding region in CREB, bacterially purified recombinant Jacob and CREB proteins were expressed with MBP and His-SUMO tags (Fig. S1B, C). In these assays we found an association of both N-terminal (117-172 aa) and C-terminal (262-532 aa) fragments of Jacob to the bZIP domain of CREB (Fig. S1B, C).

We next studied a direct interaction in living cells using Jacob fused with GFP and CREB fused with tagRFP that were co-expressed as fluorescence resonance energy transfer (FRET) pairs (Fig. 1E-I). In support of the data from pull-down assays we found significant *in vivo* FRET efficiency when we co-transfected either full-length or the N-terminal half of Jacob as well as a C-terminal fragment of CREB (Fig. 1F-I). Of

note, the N-terminal fragment of Jacob yields significantly stronger FRET signals than the C-terminal fragment (Fig. 1G-J).

LMO4 is a direct binding partner of Jacob.

In a yeast two-hybrid (YTH) screen performed with the N-terminus of Jacob as bait we identified LMO4 as a binding partner (Fig. 2A). LMO4 has been shown to be a transcriptional co-activator of CREB (33). We, therefore, wondered whether the Jacob-LMO4 interaction has a role in Jacob-induced CREB shut-off.

We first further characterized the interaction using the YTH system (Fig. 2A) where we found that a region encompassing aa 117-228 of Jacob interacts with the LIM1 domain of LMO4 (Fig. 2A). Pull-down assays where GST-LMO4 was coupled to the beads revealed a direct interaction with the N-terminus of Jacob (Fig. 2B, Fig. S1A, Fig. S2A). Furthermore, we could detect both endogenous proteins in close proximity to each other in neuronal nuclei with STED-resolution (Fig. 2C, D). We also found co-localization of the LIM1 domain with cytosolic Jacob clusters following heterologous expression, supporting the finding that the N-terminus of Jacob interacts with the LIM1 domain of LMO4 (Fig. 2E). The association between the LIM1 domain and the N-terminus of Jacob was further confirmed by heterologous co-immunoprecipitation with tag-specific antibodies (Fig. 2F) and a direct interaction was corroborated by *in vivo* FRET analysis (Fig. 2G-I). Heterologous co-immunoprecipitation of Jacob fragments with the LIM1 domain suggests that the binding interfaces for LMO4 and CREB do not overlap (Fig. 2J). Previous studies suggest that binding regions for LMO4 frequently contain hydrophobic amino acids and particularly leucine (L) and valine (V) are crucial for the binding interface (34). Jacob contains a leucine-rich stretch of amino acids between 173-228 aa (Fig. 2K). When we introduced corresponding point mutations (L175A-V176A) we found that the mutant protein indeed exhibited clearly weaker binding (Fig. 2K-M). We have previously shown that myristoylation-deficient Jacob accumulates in neuronal nuclei and leads to dephosphorylation of CREB (27). Interestingly, nuclear overexpression of the LMO4 binding mutant of Jacob did not induce CREB shut-off (Fig. 2N-P), indicating that the association with LMO4 is instrumental for Jacob-induced dephosphorylation of CREB.

LMO4 is a direct binding partner of CREB

The presence of LMO4 in the CREB complex has been proposed previously (33). However, a direct interaction between both proteins has not been shown yet. Therefore, we investigated next whether LMO4 and CREB can directly interact with each other. First evidence for this notion came from *in vivo* FRET assays where we found that the LIM1 domain, which is also the binding interface for Jacob (Fig. 2E-J), interacts with a C-terminal fragment of CREB (Fig. 3A-C). Pull-down revealed that LMO4 directly binds to this region but not like Jacob, the bZIP domain of CREB alone (Fig. 3D-F, Fig. S2A, B). Expression of LMO4 in HEK293T cells increases CRE-driven luciferase activity (Fig. 3G). Interestingly, shRNA knockdown of LMO4 in neurons reduces nuclear pCREB immunofluorescence (Fig. 3H, I, Fig. S2C-E) but not total CREB levels (Fig. 3J, K). Collectively these data indicate that the direct interaction with LMO4 promotes phosphorylation of Ser133 and thereby CREB transcriptional activity.

Jacob, CREB and LMO4 can assemble in a triple complex in living cells and Jacob competes with CREB for LMO4 binding

Direct binding of LMO4 to CREB and Jacob raises the question whether all three proteins can assemble in a trimeric complex or whether they compete for the same binding interface. To study this question we first employed sequential resonance energy transfer (SRET), a technique that is well suited to study triple protein complexes in living cells (35). Indeed, SRET revealed the existence of a triple complex of Jacob, CREB and LMO4 (Fig. 4A, B). Jacob harbors a binding interface for the interaction with CREB and LMO4 at the N-terminus (Fig.1, 2) whereas LMO4 can only associate with the first LIM domain either to Jacob or to CREB (Fig. 2, 3). The second LIM domain contributes to formation of a LMO4 dimer. Subsequent competition pull-down experiments confirmed competitive binding between the N-terminus of Jacob and CREB with LMO4 when GST-LMO4 was coupled to the beads and increasing amounts of the N-terminal fragment of Jacob were added in the presence of CREB (Fig. 4C-E). These data suggest that the LIM1 domain of LMO4 will either associate with CREB or with Jacob and that Jacob is capable to displace LMO4 from the CREB complex (Fig. 4C-E), a mechanism that should facilitate CREB shut-off.

PP1γ binds to nuclear Jacob and is involved in Jacob-induced CREB shut-off

Previous reports have shown the involvement of PP1 in NMDA-induced CREB shut-off (35). A closer inspection of Jacob's primary structure reveals the presence of

several PP1 binding motifs that are present in many PP1 regulators like neurabin 1, inhibitor-1 and inhibitor-2 (36-39). PP1γ and Jacob show extensive co-clustering following heterologous expression (Fig. 5A) and tagged Jacob co-immunoprecipitates with endogenous PP1γ when immunoprecipitated with a tag-specific antibody (Fig. 5B). In pull-down experiments, we established a direct interaction of bacterially expressed recombinant proteins (Fig. 5C, Fig.S3A). Of note, heterologous co-immunoprecipitation experiments revealed two binding interfaces for association with PP1γ (Fig. 5D, E). We next addressed whether the association with PP1γ is crucial for Jacob-induced CREB shut-off. To this end we expressed a phosphodeficient mutant of Jacob in the nucleus of hippocampal primary neurons (28) and incubated the cultures with 2 µM okadaic acid (OA) to inhibit PP1γ phosphatase activity. We found that treatment with OA prevented Jacob-induced CREB shut-off (Fig. 5F, G).

Interaction of Jacob with LMO4 depends on serine 180 phosphorylation

Phosphorylation of Jacob at serine 180 is induced by activation of synaptic NMDAR, whereas nuclear import of the non-phosphorylated protein is related to activation of extrasynaptic NMDAR (28). Accordingly, in a CRE-luciferase activity assay the expression of wild-type but not phosphodeficient Jacob causes an increase in CRE-dependent luciferase activity (Fig. 6A, Fig. S3C). Taken together the data so far indicate that Jacob associates with CREB irrespective of Ser180 phosphorylation, but only in case of Ser180 phosphorylation Jacob will enhance transcriptional activity of CREB. We, therefore, next asked whether the association of Jacob with LMO4 depends on Ser180 phosphorylation. We observed that a phosphodeficient mutant of Jacob associated significantly stronger with LMO4 than the phosphomimetic protein (Fig. 6B, C, Fig. S3C). Accordingly, phosphomimetic Jacob, unlike the non-phosphorylated protein, did not displace CREB from LMO4 bound to the beads (Fig. 6D, E, Fig. 4D, E). To further test the notion that LMO4 binds to non-phosphorylated Jacob more efficiently we applied the protein kinase inhibitor staurosporine and performed heterologous co-immunoprecipitation experiments (Fig. 6F+G). In these experiments, we indeed found a stronger association of non-phosphorylated Jacob to LMO4 (Fig. 6F) and concomitantly a stronger association of Ser180 phosphorylated Jacob to CREB (Fig. 6G). Since Jacob directly interacts with PP1γ (Fig. 5C) we next performed a pull-down assay where we found that the association between both proteins became even stronger in the presence of LMO4 (Fig. 6H-J, Fig. S3D, E). This

supports the idea that non-phosphorylated Jacob, entering the nucleus following activation of extrasynaptic NMDAR, will displace LMO4 from the CREB complex and its association with LMO4 will further enhance binding to PP1γ.

Jacob protein knockdown reduces NMDA-induced CREB shut-off

The displacement of LMO4 from CREB and a subsequent enhanced association with PP1γ provides a conceivable mechanism for Jacob-induced CREB shut-off. We therefore next investigated the role of Jacob in NMDA-induced CREB shut-off in mature hippocampal neurons (DIV16) in more detail. To this end, we employed primary cultures that were silenced using TTX to block spontaneous activity. Next, the neuronal activity was boosted by the application of forskolin with simultaneous blocking of non-NMDA Ca^{2+} channels by CNQX and nifedipine. pCREB levels were monitored after bath application of NMDA for different periods of time (Fig. S4A). In accord with previous work (27), protein knockdown of nuclear Jacob significantly rescued NMDA-induced CREB shut-off in hippocampal primary neurons after 5, 10, and 15 minutes of bath application of NMDA (Fig. S4A-C).

Therefore, we hypothesized that the lack of Jacob could prevent neuronal cell death. To address this question, we compared the propidium iodide (PI) uptake after oxygen-glucose depravation (OGD) or NMDA-induced cell death in organotypic hippocampal slice cultures from Jacob/*Nsmf* -/- animals and wild-type littermates (Fig. S5). PI is a red-fluorescent nuclear counterstain not permeant to living cells, thus the increase in fluorescence provides a read out of cell death. Both, oxygen-glucose deprivation (Fig. S5A-E), and treatment with 50 µM NMDA (Fig. S5F-I) induced massive cell death in DG, CA3, and CA1 region of hippocampus already after 3h (Fig. S5A-I). In case of NMDA-treatment cell death could be blocked by co-application of the NMDAR antagonist MK-801 (40) (Fig. S5J, K). However, we could not see any difference between genotypes in PI uptake at any of the investigated time points (Fig. S5). Thus, Jacob-induced CREB shut-off is not relevant in neurodegeneration induced by acute excitotoxic insults.

Jacob/*Nsmf* gene knock out protects against amyloid-β toxicity

Since the studies above indicate that deletion of the Jacob/*Nsmf* gene does not confer neuroprotection in ischemia or acute NMDA-induced excitotoxicity in

organotypic slices we wondered whether CREB shut-off might gain more pathophysiological relevance in slowly progressing disease states like for instance AD. CREB shut-off is a hallmark of AD (18, 19, 21-25) and our previous studies indicate that Jacob plays a role in Aβ-induced CREB shut-off that is elicited by activation of extrasynaptic GluN2B containing NMDAR (30-32). In the brain of AD patients, Aβ oligomers can be found in various, post-translationally modified forms (41), out of which the N-terminally truncated, pyroglutamylated $A\beta_{3(pE)-42}$ species are very prominent (42-47). $A\beta_{1-42}$ and $A\beta_{3(pE)-42}$-induced CREB shut-off cause the impairment of synaptic function with subsequent synapse loss via different pathways that converge on nuclear import of nonphophorylated Jacob (31). In accordance with this previous work shRNA knockdown of Jacob (27) in hippocampal neurons prevented CREB shut-off induced by treatment of cultures with 500 nM $A\beta_{1-42}$ or $A\beta_{3(pE)-42}$ as evidenced by quantification of pCREB nuclear immunofluorescence intensity (Fig. 7A, B). To further investigate the role of Jacob in Aβ-induced CREB shut-off, we treated organotypic hippocampal slices from Jacob/*Nsmf* knock out mice or WT littermates with 1 µM of $A\beta_{1-42}$ oligomers (Fig. 7C-F). Basal pCREB nuclear immunofluorescence levels were not different between both genotypes, however, following incubation with $A\beta_{1-42}$ oligomers, neurons from Jacob/*Nsmf* mice did not display CREB shut-off when compared the slices from WT mice (Fig. 7C, D). Total CREB levels remained unchanged following acute treatment with $A\beta_{1-42}$ oligomers in slices from both genotypes (Fig. 7E, F).

Jacob/*Nsmf* gene knock out ameliorates neuronal loss in AD mice

Next, we hypothesized that the lack of Aβ-induced CREB shut-off in organotypic slices derived from Jacob/*Nsmf* knock out mice should confer neuroprotection in AD. TBA2.1 mice express $A\beta_{3(pE)-42}$ under control of a Thy-1 promoter (48). The CA1 subfield of the hippocampus is one of the earliest areas affected in AD, with pronounced neuronal loss, decreased number of synaptic contacts, and the aggregation of hyperphosphorylated Tau (49-53). Likewise, TBA2.1 mice display severe CA1 neuronal loss, amyloidosis, LTP impairment, and neuroinflammation (48).

First, we assessed the phosphorylation status of Jacob in the CA1 region of these mice in comparison to wild-type littermates. Western blot analysis of protein extracts revealed unchanged Jacob protein levels (Fig. S6A, D), however, significantly decreased pJacob levels and a reduced pJacob/Jacob ratio (Fig. S6B-D). These

results are in line with previous evidence showing that amyloid-β oligomers induce translocation of non-phosphorylated Jacob to the nucleus (30-32).

To study whether the loss of Jacob expression in neurons confers neuroprotection we next crossed homozygous TBA2.1 and Jacob/*Nsmf* -/- mice. It has already been shown that in 12 weeks old homozygous TBA2.1 mice display cell loss of CA1 neurons and pronounced neuroinflammation when compared to wild-type animals (48). In accordance with reports from other AD mouse lines (24-26), we found that TBA2.1 mice exhibit significantly less nuclear pCREB levels when compared to wild-type animals (Fig. 8A-C). Interestingly, the double transgenic animals (TBA2.1 x Jacob/*Nsmf* -/-mice), did not display reduced pCREB (Fig. 8A-C). Although we observed in all three genotypes (TBA2.1, Jacob/*Nsmf* -/-, and double transgenic animals) slightly decreased total nuclear CREB levels as compared to wild-type mice (Fig. 8D-F), the lack of CREB shut-off in Jacob/*Nsmf* knock out and double transgenic make a strong case for a key role of Jacob in CREB shut-off at an early stage of AD. Moreover, the cell loss in the dorsal CA1 region of TBA2.1 as evidenced by NeuN-positive cell counts, was by far less pronounced in double transgenic mice (on average 23%) (Fig. 8G). These results suggest that the rescue of CREB shut-off in AD transgenic mice by gene deletion of Jacob/*Nsmf* directly correlates with ameliorated neuronal loss (Fig. 8). Finally, Jacob/*Nsmf* gene deletion does not influence the number of astrocytes (GFAP staining, Fig. S6E, F) and activated microglia (Iba-1 staining, Fig. S6E, G), which indicates that the neuroinflammatory processes in both TBA2.1 mice and double transgenic animals is comparable (Fig. S6E-G). Moreover, amyloid load as evidenced by the number of Aβ-positive plaques visualized by 4G8 staining (Fig. S6H, I) was not affected by removal of the Jacob/*Nsmf* gene.

pJacob levels are significantly decreased in the brain of AD patients

Collectively these results indicate that neither indirect effects on neuroinflammation nor amyloid deposition account for the neuroprotection conferred by gene deletion or protein knock down of Jacob. Furthermore, it is likely that Jacob-induced CREB shut-off plays a role in AD pathology. Therefore, we decided to examine the levels of pJacob and Jacob in nuclear-enriched protein extracts from post mortem tissue of temporal cortex from AD patients (see Supplementary Table 1 for information about the human subjects). Similar to TBA2.1 mice (Fig. S6 A-D), immunoblots from a nuclear enriched fraction obtained from the temporal cortex of 12 AD patients and 11

corresponding controls did not reveal a significant reduction in total Jacob levels (Fig. 9A, E; Fig. S7A, B). However, the levels of pJacob were significantly decreased by roughly 40% (Fig. 9B, E; Fig. S7A, C), indicating that nuclear import of Jacob following activation of synaptic NMDAR is diminished probably at the expense of activation of the extrasynaptic NMDAR pathway. In accordance with previous reports (54), we could observe significant neuronal loss in AD patients as evidenced by NeuN-immunoblotting (Fig. 9C, E). Jacob is, unlike CREB, exclusively expressed in neurons (55). We next compared the phosphorylation status of nuclear Jacob normalized to total protein levels and corrected these values for NeuN content to adjust for neuronal cell loss (Fig. 9D, E). We observed a clear reduction of pJacob/Jacob ratio (Fig. 9D, E), which further supports the notion that Jacob in AD patients will be likely upstream of CREB shut-off.

Discussion

AD patients display reduced pCREB levels in the prefrontal cortex (56) and hippocampus (57, 58), and a central role of CREB shut-off in early AD pathology has already been suggested in numerous studies (11, 21, 22, 24, 59, 60). The molecular mechanisms underlying CREB shut-off, however, are largely unknown (19, 61). The present work proposes a novel pathway implying extrasynaptic NMDAR and nuclear import of Jacob for the induction of CREB shut-off. First, we provide evidence that Jacob directly associates with the bZIP domain of CREB. We could next show that binding of an adaptor protein determines whether Jacob associates with the CREB phosphatase PP1γ or ERK-kinase, which in turn is decisive whether Jacob induces CREB shut-off or enhanced CREB-dependent gene transcription (Fig. S8). In consequence, we assume that activation of synaptic or extrasynaptic NMDAR will determine which type of signalosome Jacob will dock to the CREB complex and it is tempting to speculate that Jacob assembles a membrane proximal signalosome that differs between synaptic and extrasynaptic NMDAR (Fig. S8). In this scenario long-distance trafficking of Jacob delivers the signalosome piggyback to the nucleus and docks it to CREB by a direct interaction. Moreover, once in the nucleus Jacob is also capable to displace LMO4 from the CREB complex (Fig. S8), a second mechanism that might further contribute to long-lasting CREB dephosphorylation. Thus, enhanced binding of Jacob to PP1γ and displacement of the co-activator LMO4, makes the association with LMO4 a key event for Jacob-induced CREB shut-off.

Interestingly, we found that Jacob-induced CREB shut-off is not relevant for acute excitotoxicity and cell death. This might be explained by the fact that lack of CREB-dependent pro-survival and plasticity-relevant gene expression will not immediately induce synaptic dysfunction and is not causative for instantaneous cell death like for instance breakdown of the mitochondrial membrane potential (16). Jacob-induced CREB shut-off kicks in at later time points when extrasynaptic NMDAR stimulation by agents like oligomeric amyloid-β is slow but continuous and results in chronic cellular degeneration induced by altered gene transcription. Thus, the data suggest that Jacob is a regulator of long-lasting CREB shut-off under conditions of neurodegeneration like it occurs in AD. A number of intriguing questions derive from these findings that we want to discuss below.

A novel mechanism for CREB shut-off in AD

We could show in this study that LMO4 directly binds to CREB. LMO4 is a downstream mediator of neuroprotective effects of extracellular ATP, it can prevent neuronal death after ischemia in cortical neurons (62, 63) and it has been shown to be a transcriptional co-activator of CREB (33). Our data suggest that LMO4 will likely hinder dephosphorylation of S133, stabilize the CREB dimer and thereby act as a transcriptional enhancer. Of note, LMO4 is an adaptor protein belonging to the LIM domain-containing family of transcriptional co-factors and regulates the transcriptional activity of various transcription factors (33, 64-69). This in turn raises the possibility that due to its binding to LMO4 Jacob might be part of other transcriptional complexes in the nucleus.

Detailed mapping of the binding regions revealed that Jacob harbors two different binding sites at the N- and the C-terminus of CREB. Furthermore, both Jacob and CREB can directly bind to the LIM1 domain of LMO4 and this might result in the displacement of LMO4 from CREB by Jacob (Fig. S8). The N-terminal half of Jacob that contains the LMO4 binding interface as well as a PP1γ binding site (Fig. S8) is sufficient to induce CREB shut-off (27) and this points to the importance of LMO4 for Jacob-induced transcriptional inactivation of CREB. The C-terminal half lacks such activity, despite an association with PP1γ and CREB, which is though considerably weaker. In summary, binding and potentially displacement of LMO4 via the N-terminus of Jacob is a first crucial step for CREB shut-off. Since okadaic acid treatment abolishes Jacob-induced CREB shut-off we propose that docking of PP1γ in a manner

facilitated by LMO4 is the second mechanism of Jacob-induced CREB shut-off in neurodegeneration. Jacob can directly interact with PP1γ, which is mainly concentrated in the cell body and the nucleus (70). A major substrate of PP1γ in the nucleus is the transcription factor CREB (71). In addition to phosphorylation, PP1γ phosphatase activity is regulated by a large and growing number of targeting subunits, as well as by a smaller number of inhibitor proteins that interact with PP1γ in a mutually exclusive manner (72-74). An open question, therefore, is whether Jacob might also displace an inhibitor from PP1γ and thereby regulate its activity or whether it serves exclusively as a targeting activating subunit. Finally, irrespective whether the Jacob-PP1γ complex will assemble at the plasma membrane or in the nucleus this mechanism will contribute to signaling downstream of extrasynaptic NMDAR (Fig. S8).

The pathophysiological role of CREB and the Jacob-signalosome in AD

The CA1 region of the dorsal hippocampus is among the first to exhibit AD pathology in humans. Moreover, it shows deficits in CREB activation, neuronal complexity, and neuronal network activity in both human patients and mouse AD models (24-26, 48, 50-52, 56, 57, 75). Increasing pCREB levels in the CA1 region of AD mice improves spatial memory, and reverses the deficits in dendritic arborization and neuronal network activity (24, 26). The results of this rescue closely mirrors those of previous studies in which synaptic pathology was reversed by restoring CREB function through agents such as rolipram (76, 77) or its analogue GEBR-7b (78). Interestingly, the improvement in spatial memory occurred independently of amyloid-β plaque load and might be related to the extent of synapse loss, which is a more robust correlate of cognitive impairment in AD patients at an early stage than amyloid–β or neurofibrillary tangle pathology (56, 77-79). Thus, measures to enhance CREB activity might restore learning and memory through compensatory mechanisms that circumvent amyloid-β pathology. In previous work we found that one of the earliest phenotypes following nuclear accumulation of non-phosphorylated Jacob is the stripping of synaptic contacts (27, 28). Given that the most promising therapeutic window is before the onset of the disease, right at the time of beginning synaptic dysfunction, this is an interesting observation and Jacob is therefore an attractive target for interventions to promote plasticity. In fact, interventions are conceivable that will drive the nuclear import of a synaptic Jacob-signalosome to counteract CREB shut-off and improve cognition. For example, rolipram might induce ERK-dependent

phosphorylation of Jacob at S180 and thereby counteract the deleterious effects of Aβ and activation of extrasynaptic NMDAR.

On the other hand, preventing the formation of Jacob signalosomes related to extrasynaptic GluN2B-containing NMDAR activation could further minimize the Aβ-induced CREB shut-off. It was shown previously that administration of memantine, a drug that preferentially inhibits extrasynaptic NMDAR (80), alleviates the symptoms in patients with moderate-to-severe disease progression (81). Furthermore, memantine rescued synaptic depression by abolishing extrasynaptic NMDAR-induced synaptic impairment (11). Interestingly, memantine was also shown to enhance CREB phosphorylation and to restore cognitive function (82). Based on these reports and the results of the present study, it is tempting to speculate that the beneficial effects of memantine in AD result at least in part mediated by reduced nuclear translocation of Jacob from extrasynaptic NMDAR. Thus, we propose that the underlying mechanism of Jacob-induced CREB shut-off is a promising therapeutic target.

Materials and methods

Contact for reagent and resource sharing

Further requests and queries should be addressed to and fulfilled by the Lead Contact, Michael R. Kreutz (kreutz@lin-magdeburg.de).

Experimental models and subject details

Animals

Animals used in the experiments were maintained under controlled environmental conditions in the animal facility of the Leibniz Institute for Neurobiology, Magdeburg, Germany or Center for Molecular Neurobiology Hamburg, Germany. Jacob/*Nsmf* knock out animals were characterized before (83). The TBA2.1 mice (48) were a kind gift from ProBiodrug. This AD mouse model overexpresses the Aβ3(pE)-42 peptide driven by a Thy-1 promoter. The upstream sequence coding for pre/pro-peptide of the murine thyrotropin-releasing hormone leads to cleavage within the trans-Golgi and vesicular secretion of Aβ3(pE)-42 (48).

To generate the double transgenic animals (TBA2.1, -/-) the Jacob/*Nsmf* heterozygous mice were crossed with heterozygous TBA2.1 mice. The F1 generation was crossed to obtain homozygous Jacob/*Nsmf* knock out and TBA2.1 animals, as

well as littermates that were used as controls (WT, Jacob/*Nsmf* knock out, TBA2.1). All lines had a C57BL/6 background.

Genotyping of *Jacob*/TBA2.1 mice

Genotyping was performed using standard PCR protocols on tail biopsies after lysis in a tail-cut buffer (10 mM Tris HCl pH 8.0, 100 mM NaCl, Proteinase K - 0,4 mg/ml) with the following primers for TBA2.1: TBA-12-for: TGCCCATATGTCCTAAGCTC, TBA-13-rev: CAGCTTCCATGGCAGTATTT, TBA-15-for: GGCATGACAGATACCAAAGC (48). Primers for confirming the deletion of Jacob/*Nsmf* gene were described previously (83).

Case recruitment and characterization of human brain tissue

The temporal cortex (area 22) biospecimens were provided by the former Brain Banking Centre Leipzig of the German Brain-Net, operated by the Paul Flechsig Institute of Brain Research, Medical Faculty, University of Leipzig. The diagnosis and staging of AD cases used in this study was based on the presence of neurofibrillary tangles (53) and neuritic plaques in the hippocampal formation and neocortical areas as outlined by the Consortium to establish a registry for AD (CERAD; (84)) and met the criteria of the National Institute on Aging (NIA) on the likelihood of dementia (The National Institute on Aging, 1997). Brain tissue of temporal cortex (Area 22) from 12 controls and 11 age-matched AD cases (Supplementary Table 1) was used for biochemical analyses.

Method details

cDNA constructs, shRNA, recombinant proteins and antibodies

A list with the main constructs used in this study and their source is available in Suppl. Table 2.

Yeast Two-Hybrid

The Yeast-Two-Hybrid screening for Jacob interaction partners was performed using a transformed human brain cDNA Library in pACT2 (Matchmaker-GAL4 Two-Hybrid II; Clontech) as described previously (87). The yeast strains AH109 and Y187 (both from Clontech) were used. The Jacob-LMO4 interaction was confirmed using the bait vector pGBKT7 and the prey vector pGADT7 deriving from the MATCHMAKER Two-

Hybrid System 3 (Takara/Clontech,). Jacob constructs of various lengths were fused with the Gal4 DNA binding domain while LMO4 and the two individual LIM domains, LIM1 and LIM2, were fused to the Gal4 activation domain. Co-transformed yeasts were assayed for growth on quadruple drop-out medium (SD/–Ade/–His/–Leu/–Trp) and additionally for LacZ reporter activation accordingly to the manufacturer's instructions.

Biochemistry

Heterologous co-immunoprecipitation

HEK293T cells, grown in 10 ml flasks were transfected via calcium phosphate DNA precipitation method. Cells co-expressing full-length Jacob-GFP, Jacob mutants and short fragments of Jacob tagged with GFP together with tRFP tagged LMO4 as well as with mCherry-PP1γ were harvested and lysed in 1ml of RIPA buffer containing 50 mM Tris-HCl pH 7.4, 150 mM NaCl and 1% Triton X-100, 0.5% sodium deoxycholate, 0.1% sodium dodecyl sulfate (SDS), protease inhibitors (Complete, Roche, Cat#04693159001) and PhosphoStop (Roche, Cat#04906837001) for 1h at 4°C. For co-immunoprecipitation of endogenous CREB with the Jacob-GFP, the following lysis buffer was used: 50 mM TRIS, 150 NaCl, 1% NP-40, 0,1% SDS, protease inhibitors (Complete, Roche, Cat#04693159001), PhosphoStop (Roche, Cat#04906837001). All samples were ultrasonicated for 30 sec three times, lysates were cleared by centrifugation for 20 min at 20000g, at 4°C and incubated with anti-GFP antibody-coated magnetic beads (MultiMACS GFP Isolation Kit, Cat#130-094-253) for 90 min at 4°C. The co-immunoprecipitation was performed following the manufacturer’s protocol. All magnetic columns were washed three times with corresponding lysis buffer, rinsed with 200 µl of 20 mM TRIS and the immunocomplex was eluted with 50 µl of 95°C 2xSDS sample buffer (250 mM Tris-HCl, pH 6.8, 1% (w/v) SDS, 40% (v/v) Glycerol, 20% (v/v) β-mercaptoethanol, 0,004 % Bromophenol Blue). The proteins were separated by 5-20% gradient SDS-PAGE and analyzed by western blotting (WB).

The phospho-dependent association of overexpressed nuclear Jacob (ΔMyr-Jacob-GFP) with either CREB-tagRFP or LMO4-tagRFP was assessed by heterologous co-immunoprecipitation assays where HEK293T cells overexpressing above-mentioned constructs were pre-treated with 20 nM of staurosporine (Tocris, Cat# 1285) for 3 h.

Details about antibodies used for protein detection are listed in the supplement table 2.

Fluorescence resonance energy transfer (FRET) assays and sequential resonance energy transfer (SRET) assays in HEK293T cell suspension

For FRET experiments, HEK293T cells were transiently co-transfected with different combinations of two genes of interest (Jacob-GFP:CREB-1-165-tagRFP; Jacob-GFP:CREB-166-341-tRFP; Jacob-1-228-GFP:CREB-tagRFP; Jacob-262-532-GFP:CREB-tagRFP; Jacob-1-228-GFP:LMO4-tagRFP; Jacob-262-532-GFP:LMO4-tagRFP; Jacob-GFP:LIM1-1-80-tagRFP; Jacob-GFP:LIM2-81-165-tagRFP; LMO4-GFP:CREB-1-165-tagRFP; LMO4-GFP:CREB-166-341-tRFP; CREB-GFP:LIM1-1-80-tagRFP; CREB-GFP:LIM2-81-165-tagRFP) tagged with donor (GFP) and acceptor (tagRFP) fluorophores. The concentration of cDNA encoding GFP-tagged genes remained constant throughout the experiments, however, the amount of tagRFP expressing plasmid was increased to ensure raising levels of protein expression to reach the binding saturation. Plasmids expressing only GFP and tagRFP, as well as Caldendrin (CDD-GFP) were used as a negative and non-related protein controls accordingly. FRET was performed as described previously (88). For SRET measurements, 48 h post-transfection cells were resuspended in Hank´s balanced salt solution (HBSS) supplemented with 10 mM glucose (Sigma-Aldrich). 100 µl aliquots of triple construct-transfected (CREB-Rluc:Jacob-GFP:LMO4-tagRFP) cell suspension containing 20 µg of total protein were used to perform the three distinct measurements for the assessment of the SRET efficiency. (i) Firstly, the LMO4-tagRFP protein expression level was quantified by determination of the tagRFP fluorescence intensity. Briefly, transfected cells were loaded into 96-well black microplates with a transparent bottom and emission intensity of tagRFP was measured by the FLUOstar Optima Fluorimeter (BMG Labtechnologies) equipped with a high-energy xenon flash lamp, an excitation filter at 530 nm, and 30 nm bandwidth emission filters corresponding to 590 nm (575-605 nm). Subsequently, the sample fluorescence intensity of the LMO4-tRFP was calculated by subtracting the control fluorescence intensity performed for cells expressing CREB-Rluc:Jacob-GFP:LMO4-Myc from the fluorescence intensity measured in the presence of the FRET acceptor. (ii) Secondly, the CREB-Rluc expression level was estimated by CREB-Rluc luminescence upon addition of renilla luciferase substrate. Briefly, the

cell suspension was loaded into 96-well white plates with a white bottom (Corning 3600) and CREB-Rluc luminescence was determined 10 min after addition of coelenterazine H (5 µM) using a Mithras LB 940 multimode microplate reader (Berthold Technologies). (iii) For SRET measurements cells from the same samples were loaded into 96-well white plates with a white bottom (Corning 3600) and 5 µM of coelenterazine derivative DeepBlueC (Molecular Probes, Eugene) that serves as a substrate for Renilla luciferase and generates an emission peak centered around 400 nm, was added. SRET signal was collected using Mithras LB 940 equipped with the detection filters at short-wavelength at 400 nm (370-450 nm) and at long-wavelength at 590 nm (510-590 nm). Net SRET was defined as [(long-wavelength emission)/(short-wavelength emission)]-Cf, where Cf corresponds to [(long-wavelength emission)/(short-wavelength emission)] for cells expressing CREB-Rluc:Jacob-GFP:LMO4-Myc (similar values were obtained measuring Cf in cells expressing only protein-Rluc and protein-GFP).

Expression and purification of recombinant proteins

GST-, MBP- and his-SUMO- tagged recombinant proteins were produced and purified as described previously (27, 28). Briefly, the desired DNA sequence was subcloned into pGEX, pMAL-c5X or pET-His-SUMO vectors. Then, competent E.coli BL21 (DE3) or SHuffle (T7) Express lysY cultures were transformed with corresponding vectors, grown in LB media and induced with IPTG (0.4-1mM) for 2 h to overnight at temperatures ranging from 16ºC to 37ºC. Bacterial pellets were lysed using French press (15,000 Pa) followed by ultrasonication in the presence of 0.1% Triton X-100. For GST-LMO4 protein production, LB media containing 1% glucose and 4% sucrose was used and bacterial cultures were induced with 400 mM IPTG followed by overnight incubation at 16°C post induction. Lysates were spun down at 13,000 rpm for 30 min at 4ºC. All proteins were purified from the soluble fraction by affinity chromatography using glutathione sepharose (GE health care) or glutathione agarose (Protino, Machery Nagel) for GST tagged, amylose resin (NEB) for MBP tagged, and probond resin (Invitrogen) for SUMO tagged proteins.

Pull-down assays

Pull-down assays used to assess the direct interaction between Jacob, CREB, LMO4, as well as Jacob with PP1γ and further to map their binding interfaces were

performed as described previously (27, 28, 89). Briefly, protein amounts ranging from 1-10 µg along with the equivalent amount of the control tag protein was bound on the respective beads and incubated with 5% BSA for 1 h at room temperature (RT). 100 ng-10 µg of the second recombinant protein was incubated with the resin bound protein in 1 ml TBS buffer (25 mM TRIS pH=7.4, 50 mM NaCl) for 1h either at RT or 3 h at 4°C. After three washing steps with TBS (25 mM TRIS pH=7.4, 50 mM NaCl, 0,1% TritonX-100) buffer, the complex was eluted in 2X SDS sample buffer and subjected to WB.

Competition pull-down assay

Competition pull-down assays with recombinant MBP-Jacob-45-228 and 6xHis-SUMO-CREB or GST-LMO4 were performed as described previously (89). Briefly, 10µg of GST-LMO4 and equivalent amounts of GST control protein were bound to glutathione beads followed by blocking with 5% BSA and washing. Firstly, His-SUMO-CREB was incubated with GST-LMO4 and GST control protein immobilized on beads for 5 min at 4°C. Then, recombinant Jacob protein was added into the protein mix in different ratios compare to His-SUMO-CREB amount: MBP-Jacob-45-228 - 1:1, 1:4 and 1:8 and incubated for additional 25 minutes at 4°C. Probes were eluted with 20µl of 2x SDS sample buffer after incubation and washing steps (wash buffer: 50 mM Tris, 500 mM NaCl, 0.1% Triton-X100, Protease Inhibitor Cat#04693159001, pH 7.4), and subjected to SDS PAGE. Anti-panCREB rabbit monoclonal and anti-MBP mouse monoclonal antibodies were used for detection of recombinant proteins after western blotting.

Preparation of protein extracts from human cortex and murine CA1

Human brain samples or murine CA1 were homogenized in a buffer containing 0.32 M sucrose, 5 mM HEPES, protease inhibitors (Sigma, Cat#P8340) and phosphatase inhibitors (Roche, Cat#04906837001), in a 1g /10ml ratio. The homogenates were centrifuged at 1000 g for 10 minutes at 4ºC. The pellets were resuspended in the homogenization buffer and used for immunoblotting. The membranes were probed with antibodies detecting pan-Jacob, pJacob (pS/T180), and NeuN (all antibodies were probed on different membranes). As a loading control, each membrane was probed with anti-Histone3 antibody. The Jacob and pJacob bands intensities was quantified with Fiji software (90) and normalized to band intensity of Histone3. For

initial characterization of anti-panJacob and pJacob(S180) antibodies for the detection of human protein HEK293T cells were transfected with the plasmid expressing hJacob-SPOT. Overexpressed protein was immunoprecipitated from the cell lysate using tag specific nano-trap (SPOT-Trap-MA, Chromotek) and western blot analysis was performed for both antibodies.

Luciferase assay

Stably transfected HEK293T cell line expressing luciferase under the CRE promoter (vector pGL4.29[luc2P/CRE/Hygro], Promega) was transfected with LMO4-Myc, ΔMyr-Jacob-Myc, ΔMyr-Jacob-S180A-Myc and Myc control vector (pcDNA). On the following day, cells were lysed with the lysis buffer (25mM Tris-phosphate, 2mM DTT, 2mM 1,2-diaminocyclohexane-N,N,N´,N´-tetraacetic acid, 10% glycerol, 1% TritonX-100, pH 7.8) and the cellular extract was transferred to 96 well plate and luciferase activity was measured with the Dual-Luciferase Reporter Assay System (Promega) on a (FLUOstar Omega, BMG Labtech). The luciferase activity was normalized to the protein content in each sample. Phosphorylation of Ser180 of overexpressed in HEK293T cells nuclear Jacob was controlled by ICC with anti-pJacob antibodies.

Aβ-oligomer production

Human Aβ oligomers (Anaspec, Cat#AS-20276) were prepared and characterized as described previously (31). Briefly, the lyophilised Aβ1-42 was incubated in 1,1,1,3,3,3-hexafluoro-2propanol (HFIP, Sigma-Aldrich, Cat#B2517) to the final concentration 0.5 mg/ml. The solution was aliquoted. After that, HFIP was evaporated and the peptide film was stored at -80°C. 24 h before use, the peptide film was dissolved in DMSO (1:1000, Sigma-Aldrich, Cat#276855), sonicated, diluted to 50 µM concentration in F12 medium (Gibco; Cat#21765-029) and kept for oligomerization at 4°C for 24 h. Aβ3(pE)-42 oligomers (kind gift from Hans-Ulrich Demuth; Fraunhofer Institute for Cell Therapy and Immunology IZI, Halle) were prepared accordingly to previously established protocol (91). The peptide film was dissolved in 0.1 M NaOH, vortexed, diluted in neurobasal medium (Gibco, Cat#21103049) and 0.1 M HCl was added to a final concentration of 5 µM. Oligomers were formed during incubation for 24 h.

Lentivirus production

The lentivirus was produced in the HEK293T cell line (Lenti-X 293T, Clontech). Cells were transfected with FUGW-based transfer shRNA, psPAX2 packaging, and pVSVG pseudotyping vectors using calcium phosphate method with a molar ratio of FUGW: psPAX2: pVSVG: 2:1:1. After 12-16 h of transfection, cells were cultured in low serum DMEM (Gibco, Cat#41966-029) supplemented with 4% FBS (Gibco, Cat#10270). The virus was harvested from the culture media after 48 h by ultracentrifugation at a speed of 20000 rpm for 2h at 4°C. The virus pellet was resuspended in 100 µl of Neurobasal media by shaking at 300 rpm for 55 min. Resuspended virus was collected and spun again at 14000 rpm for 5 min. The supernatant was aliquoted and stored at -80°C.

Preparation of dissociated hippocampal and cortical cultures, transfection and stimulation

Hippocampal and cortical primary cultures were prepared from Wistar rat embryos (E18) as described (92). Hippocampal neurons were plated on 18 mm glass coverslips at a density of 60000-80000 cells/ml; neurons from cortex were plated on T75 flasks at a density of 2500000 cells per 10 ml, both coated with poly-L-lysine (Sigma-Aldrich, Cat#P2636). Cells from hippocampus were plated in DMEM (GIBCO/Life Technologies) supplemented with 10% FBS, 2 mM L-glutamine (GIBCO/Life Technologies, Cat# 25030081) and 1% of penicillin/streptomycin (PAA Laboratories). 1 h after plating DMEM was exchanged to neurobasal medium (NB) supplemented with B27 (Gibco, Cat#41966-029), 2 mM L-glutamine (and 1% of penicillin/streptomycin (PAA Laboratories). At DIV4 cultures were treated with 100 nM cytosine-D-arabinofuranoside (AraC, Sigma-Aldrich, Cat# C1768) and kept in an incubator at 37°C, 5% CO2, and 95% humidity.

Cortical neurons were plated in DMEM supplemented with 10% FBS (Gibco, Cat#10270), 2 mM L-glutamine and antibiotics (Thermo Fisher Scientific, Cat#15140122). After 1 h the medium was exchanged to BrainPhys neuronal medium supplemented with SM1 (Stem Cell kit, Cat#5792) and 0.5 mM glutamine (Thermo Fisher Scientific, Cat#25030024).

Hippocampal neuronal cultures were transfected with plasmid cDNAs using Lipofectamine™ 2000 (Thermo Fisher Scientific, Cat#11668027) following the manufacturer's instructions. For LMO4 knockdown cells were expressing shRNA for

5 days; for Jacob knockdown – 4 days. For CREB shut-off experiments (Fig. 2O-P and Fig. 5F-G) hippocampal neurons were transfected at DIV15 and fixed after 24 h of overexpression. For the experiment with okadaic acid (OA, Tocris, Cat#1136) cells were treated for 20 min with 2 µM OA or DMSO control one day post transfection.

The target sequences for LMO4 and NLS-Jacob knockdown (83) as well as scrambled controls can be are indicated in Supp. Table 2.

For Aβ-induced CREB shut-off experimentse transfected neurons were treated for 40 min with 500 nM $A\beta_{1-42}$ or $A\beta3_{(pE)-42}$ oligomeric solution. For NMDA-induced CREB shut-off experiments previously described protocol was used (35). Briefly, DIV7 cultures were infected with lentivirus carrying Jacob knockdown or scrambled construct for 12 h. At DIV16, cells were silenced overnight with 1 µM tetrodotoxin (TTX, Carl Roth, Cat#6973.1) and on the following day after TTX washout cultures were treated with 100 µM Forskolin (Biorbyt, Cat#orb8092), 10 µM Nifedipine (calcium channel blocker, Santa Cruz, Cat#sc-3589), and 40 µM CNQX (Tocris, Cat#0190). After 30 min, 100 µM of NMDA (Cat#M3262, Sigma-Aldrich) was added directly into the culture media for 2, 5, 10, and 15 min. 2xSDS sample buffer with protease and phosphatase inhibitor was directly added to the wells to stop the NMDA mediated CREB shut-off and lyse the cells. Samples were subjected for the WB analysis for CREB (S133) phosphorylation level.

Cultured murine hippocampal slices, stimulation, and immunocytochemistry

Murine, organotypic, hippocampal slice cultures (OHSC) were prepared according to previously published protocols (31, 93). Slices on were prepared from P7-P12 C57/B6J or Jacob/*Nsmf* knock out mice and plated on Millicell membranes (Merck Millipore, Cat#PICMORG50). OHSC were kept for at least one week in an incubator at 37°C, 5% CO2, and 95% humidity.

Before cell death experiments, the viability of slices was assessed by adding 2 µM propidium iodide (PI) for several h directly into the culture medium.

For oxygen-glucose deprivation (OGD)-induced cell death experiment membranes with OHSC were transferred to 1 ml OGD medium (Ringer solution with 10 mM mannitol or 10 mM glucose as a control) with 3 µM PI. Next, cultures were exposed to 10 min of 95% N_2/5% CO_2 gas flow in a hypoxic chamber (Billupsand Rothenberg) and kept in the reduced O_2 conditions for 30 min at 35ºC. Afterwards, the membranes

were moved back to their previous medium containing 3 µM PI and imaged at the indicated time points.

For NMDA-induced cell death experiment OHSC were transferred to the medium containing 50 µM NMDA (Cat#M3262, Sigma-Aldrich) and 3 µM PI. Afterwards, membranes were moved back to their previous medium containing 3 µM PI and imaged at the time points indicated in figure legend. To prove that the observed cell death is NMDAR-dependent, slices were pre-incubated with 10 µM MK-801 (Sigma-Aldrich, Cat#M107) for 1 h and during the NMDA exposure. To assess the cell death the images of red PI fluorescence and bright field images were acquired with a Zeiss Axioskop 2 with the 4x objective using Nikon NIS software. The CA1, C3, and DG regions of interest (ROIs) were defined based on the bright-field image. Mean pixel intensity was measured in grey-scale images, and individually baseline-corrected for time point 0 (directly after the experiment). The analysis was done by an experimenter blind to genotype and treatment group. For representative images, PI images of different time points were aligned using the Fiji plugin linear stack alignment with SIFT and default settings in the rigid mode. Represented images are contrast-enhanced (equally for all groups). PI uptake was imaged at the time points indicated in the figure legend.

For Aβ-induced CREB shut-off, OHSC were treated with 1 µM $A\beta_{1-42}$ oligomeric solution for 1 h, then fixed for 1h at RT in 4% paraformaldehyde (PFA)/4% sucrose and stained with NeuN and pCREB or CREB antibodies according to the following protocol. After fixation the slices were washed with PBS, permeabilized with 0.4% Triton X-100 and treated with 50 mM NH_4Cl for 30 min. Subsequently, the samples were blocked for 1 h in RT with 10% normal goat serum in PBS. Following blocking, the slices were incubated for 72 h with primary antibody dilution. Then slices were washed and subsequently incubated with secondary antibody dilution for 24h. Following the counterstaining with 4’,6-diamidino-2-phenylindole (DAPI; Vectashield, Biozol), the samples were mounted in Mowiol 4-88 (Calbiochem/Merck Chemicals).

Animal perfusion and immunohistochemistry, and image analysis

To characterize WT, TBA2.1, JKO/*Nsmf*, and TBA2.1 crossed with JKO/*Nsmf* mice, animalswere anesthetized with ketamine (Medistar, Cat#13690.00.00)-Rompun (Bayer), perfused with 0.9% NaCl, and fixed with 4% PFA in PBS for 4 min. Following dissection, the brains were post-fixed in 4% PFA in PBS overnight. Subsequently, the

brains were left for soaking first in 0.5 M sucrose, then in 1 M sucrose. The brains were snap-frozen and stored at -80ºC. 35 µm thick coronal cryosections were prepared using a cryostat (Leica CM3050S, Leica Microsystems). The free-floating sections were blocked in a blocking buffer containing 0.3% Triton X-100, 10% goat normal serum in PBS for 30 min at RT. Next, the sections were incubated with primary antibodies diluted in the blocking solution, overnight at 4ºC. Secondary antibodies diluted in blocking solution were applied for 2 h at RT. After washing, nuclei were counterstained with DAPI (Vectashield, Biozol) diluted 1:500 in PBS and brain sections were mounted in Mowiol 4-88 (Calbiochem/Merck Chemicals). For the detection of Aβ, the heat-based antigen retrieval method was used. Briefly, following permeabilization with 0.4% TritonX-100 and washing, brain sections were immersed into 10 µM sodium citrate solution (Fluka, pH=9) for 30 min at 80°C (water bath). After the subsequent washing steps, tissue samples were treated like described above.

Imaging of nuclear CREB/pCREB immunoreactivities in cryosections was performed using a Leica TCS SP5 system (Leica-Microsystems) equipped with Diode (405 nm), Argon (458, 476, 488, 496, 514 nm laser lines), Diode Pumped Solid State (DPSS, 561 nm) and HeNe (633). Images were acquired with a HCX Apo L20x water Na1.0 (Leica) objective lens. 35 µm thick hippocampal sections were imaged with constant laser/detector settings along the z-axis with 400 nm z-step were scanned in a 512 x 512 pixel format at 8-bit image depth with two times frame average at 400 Hz laser frequency. Five focal sections were obtained from the middle part of the slice in order to avoid the surface staining artefacts.

All quantifications were done within the distal CA1 of hippocampus. Fiji/ImageJ software (90) was used to calculate maximum intensity projection from five optical sections for each channel. CREB and pCREB immunoreactivity of every single nucleus present in a 100 µm stretch of distal CA1 was measured in arbitrary units of pixel intensity. ROIs were defined based on NeuN and DAPI stainings. The neuronal loss in cryosections was quantified based on NeuN staining. The number of cells was divided by the length of the measured CA1 region. For the quantification of microglia and astrocytes the number of cells based on overlaid DAPI and Iba-1 or GFAP signal was quantified within the rectangular region of interest within the distal CA1 region. Analysis of amyloid-β plaques was performed by counting the number of 4G8 positive puncta in the same CA1 region where the neuronal loss was quantified.

Immunocytochemistry

Dissociated cultures were fixed with 4% PFA/4% sucrose solution for 10 min at RT, and subsequently washed 3 times with PBS. Cells were permeabilized with 0.2% triton X-100 in PBS for 10 min, washed and incubated for one hour with blocking solution (2% glycine, 0.2% gelatin, 2% BSA, and 50mM NH_4Cl (pH 7.4)). The primary antibodies were diluted in the blocking solution (70 µl/coverslip) and incubated in a humidified chamber overnight at 4ºC. Next, the coverslips were washed and incubated with fluorophore coupled secondary antibodies diluted 1:500 in the blocking solution. After washing some cultures were counterstained with DAPI (Vectashield, Biozol) diluted 1:1000 in PBS. Coverslips were mounted with Mowiol 4-88 (Calbiochem/Merck Chemicals).

Goat polyclonal anti-LMO4 (C-15) raised against a sequence between amino acids 115-165 of LMO4 of human origin (accession# P61968; Santa Cruz) was tested for its specificity in immunocytochemistry employing shRNA based LMO4 KD and by preincubation of antibody with the corresponding blocking peptide.

For detection of Jacob-CREB and Jacob-LMO4 co-localization in STED imaging, a heat-based antigen retrieval (AR) protocol was used. This included the immersion of the cells into a 10 µM sodium citrate solution (pH=9) for 30 min at 80°C directly after cell permeabilization step. After the subsequent three washing steps with 1xPBS coverslips were proceed for the standard ICC protocol with antibodies applied sequentially to avoid cross-labeling.

Quantification of nuclear staining intensity

For quantification of nuclear staining intensity for CREB, pCREB as well as LMO4, somatic regions were sequentially scanned using the 63x objective installed in both: Leica TCS SP8-STED and Leica TCS SP5 systems. Image format was set to 1024x1024 or 512x512 with 2x frame averaging. Average intensity images from three optical sections (300 nm) were generated and intensity measurements were performed within the ROIs defined by DAPI staining. Images were analysed using Fiji (90) software. For visualization a Fire look-up-table (LUT) was applied.

Gated stimulated emission depletion (STED) microscopy

STED images for nuclear CREB, LMO4, and Jacob were obtained using a Leica TCS SP8 STED 3X equipped with pulsed White Light Laser (WLL) and diode 405 nm laser for excitation and pulsed depletion laser 775 nm and Leica HC APO CS2 100x/1.40 oil objective. Stained samples were excited by WLL at 561 for detection of Jacob (Figure 1A; anti-rabbit AbberiorStar580) and LMO4 (Figure 2C; anti-goat AlexaFluor561), as well as at 633 nm for detection of CREB (Figure 1A; anti-mouse AbberiorStar635p) and Jacob (Figure 2C; anti-rabbit AbberiorStar635p) respectively. WLL excitation at 488 nm was used for MAP2 detection (a neuronal marker) in confocal mode. Confocal images detecting DAPI were acquired with Diode 405 nm laser. The format for all images acquired was set to 1024-1024 pixels with an optical zoom ranging from 5 to 6 resulting in 20-23 nm pixel size in the two-dimensional XY-plane. The Z-step was 150 nm. Images were taken with 400 lines per second (400 Hz) and 4x line averaging. Time gates were set to 0.5 to 6 ns. STED and confocal images were deconvolved using Deconvolution wizard (Huygens Professional, SVI). First, the theoretical point spread function (PSF) based on optical microscopic parameters based on image metadata was calculated. Then, the optimized iteration method until it reached a quality threshold of 0.05 was used. Intensity profiles of Jacob and CREB, LMO4 and Jacob immunoreactivity within the nucleus were created in Fiji using the plot profile option.

Cell based co-recruitment assay

To assess the association of LMO4 with Jacob in mammalian cells, HEK293T cells plated on 18 mm coverslips were transfected with LMO4-tagRFP, LIM1-1-80-tagRFP or LIM2-81-165-tagRFP together with cytosolic Jacob-1-228-GFP lacking the nuclear localization sequence (NLS), as well as with GFP alone as a control. On the following day cells were fixed with 4% PFA, permeabilized with 0,1% TritonX-100 in 1xPBS for 10 min, stained with DAPI and mounted on standard glass slides. Z-stack with 300 nm step size was taken with 200 lines per second (200 Hz) and at least 2x frame averaging in 512-512 pixels format using a Leica TCS SP8-STED system. Maximal intensity images from three optical sections were generated for representative images. For nuclear recruitment of PP1γ into the nuclear Jacob clusters, HEK293T cells were co-transfected with nuclear Jacob (ΔMyr-Jacob-GFP) and mCherry-PP1γ. Images were acquired as described above.

Statistics

Data were represented as mean ±S.E.M. Cumulative frequency distribution of all nuclei intensities (analysis of hippocampal cryosections stained with pCREB or CREB antibody), graphs and statistical analysis were made with GraphPad Prism (GraphPad Software). To choose the appropriate statistical analysis, a normality test (Shapiro-Wilk test) was performed. The specific statistical tests used for the analysis are described in the figure legends.

Study approval

All animal experiments were carried out in accordance with the European Communities Council Directive (2010/63/EU) and approved by local authorities of Sachsen-Anhalt/Germany (reference number 42502-2-1264 LIN and 42502-2-1284 UNIMD) or of the city-state of Hamburg (Behörde für Gesundheit und Verbraucherschutz, Fachbereich Veterinärwesen) and the animal care committee of the University Medical Center Hamburg-Eppendorf.

For the study of human temporal cortex (area 22) biospecimens, the protocols, the informed consent forms and autopsies were approved (GZ 01GI9999-01GI0299).

Author contributions

MRK, AK, KMG designed the study. MRK, AK, KMG, RK wrote the manuscript. KMG, RK, GMG, RR, JB, GB, CF, SS, IRR, CS, MM, SR, GNB, AK conducted the experiments and analysed the data. MRK provided tools and reagents. All authors commented and revised the manuscript.

Acknowledgements

The authors gratefully acknowledge the professional technical assistance of M. Marunde, C. Borutzki and S. Hochmuth. We would like to thank Dr. Schilling and Probiodrug for the generous gift of the TBA2.1 mouse line. We would like to thank Dr. Głów for the help with virus production.

Supported by grants from the Deutsche Forschungsgemeinschaft (DFG) (Kr 1879/9-1/FOR 2419, Kr1879/5-1/6-1/10-1; CRC 779 TPB8; Research Training Group 2413 SynAGE), BMBF ‘Energi’ FKZ: 01GQ1421B, The EU Joint Programme—Neurodegenerative Disease Research (JPND) project STAD and Leibniz Foundation

to MRK. People Programme (Marie Curie Actions) of the European Union's Seventh Framework Programme FP7/2007-2013/under REA grant agreement no. [289581], H2020 Priority Excellent Science, Marie Sklodowska-Curie Actions (MSCA) MC-ITN NPlast. DFG CRC 779 TPB8 to AK. DAAD/CAPES scholarship and the Alexander-von-Humboldt Foundation/CAPES post-doctoral research fellowship to GMG.

References

1. Bading H. Therapeutic targeting of the pathological triad of extrasynaptic NMDA receptor signaling in neurodegenerations. *The Journal of experimental medicine.* 2017;214(3):569-78.
2. Hardingham GE, and Bading H. Synaptic versus extrasynaptic NMDA receptor signalling: implications for neurodegenerative disorders. *Nature reviews Neuroscience.* 2010;11(10):682-96.
3. Lau CG, and Zukin RS. NMDA receptor trafficking in synaptic plasticity and neuropsychiatric disorders. *Nature reviews Neuroscience.* 2007;8(6):413-26.
4. Parsons MP, and Raymond LA. Extrasynaptic NMDA receptor involvement in central nervous system disorders. *Neuron.* 2014;82(2):279-93.
5. Shan Y, Liu B, Li L, Chang N, Li L, Wang H, et al. Regulation of PINK1 by NR2B-containing NMDA receptors in ischemic neuronal injury. *Journal of neurochemistry.* 2009;111(5):1149-60.
6. Paoletti P, Bellone C, and Zhou Q. NMDA receptor subunit diversity: impact on receptor properties, synaptic plasticity and disease. *Nature reviews Neuroscience.* 2013;14(6):383-400.
7. Milnerwood AJ, Gladding CM, Pouladi MA, Kaufman AM, Hines RM, Boyd JD, et al. Early increase in extrasynaptic NMDA receptor signaling and expression contributes to phenotype onset in Huntington's disease mice. *Neuron.* 2010;65(2):178-90.
8. Okamoto S, Pouladi MA, Talantova M, Yao D, Xia P, Ehrnhoefer DE, et al. Balance between synaptic versus extrasynaptic NMDA receptor activity influences inclusions and neurotoxicity of mutant huntingtin. *Nature medicine.* 2009;15(12):1407-13.
9. Kessels HW, Nabavi S, and Malinow R. Metabotropic NMDA receptor function is required for beta-amyloid-induced synaptic depression. *Proceedings of the National Academy of Sciences of the United States of America.* 2013;110(10):4033-8.
10. Malinow R. New developments on the role of NMDA receptors in Alzheimer's disease. *Current opinion in neurobiology.* 2012;22(3):559-63.
11. Talantova M, Sanz-Blasco S, Zhang X, Xia P, Akhtar MW, Okamoto S, et al. Abeta induces astrocytic glutamate release, extrasynaptic NMDA receptor activation, and synaptic loss. *Proceedings of the National Academy of Sciences of the United States of America.* 2013;110(27):E2518-27.
12. Kalkhoven E. CBP and p300: HATs for different occasions. *Biochemical pharmacology.* 2004;68(6):1145-55.
13. Yamamoto KK, Gonzalez GA, Biggs WH, 3rd, and Montminy MR. Phosphorylation-induced binding and transcriptional efficacy of nuclear factor CREB. *Nature.* 1988;334(6182):494-8.
14. Barco A, Alarcon JM, and Kandel ER. Expression of constitutively active CREB protein facilitates the late phase of long-term potentiation by enhancing synaptic capture. *Cell.* 2002;108(5):689-703.
15. Carlezon WA, Jr., Duman RS, and Nestler EJ. The many faces of CREB. *Trends in neurosciences.* 2005;28(8):436-45.
16. Hardingham GE, Fukunaga Y, and Bading H. Extrasynaptic NMDARs oppose synaptic NMDARs by triggering CREB shut-off and cell death pathways. *Nature neuroscience.* 2002;5(5):405-14.
17. Dragunow M. CREB and neurodegeneration. *Frontiers in bioscience : a journal and virtual library.* 2004;9:100-3.

18. Saura CA, and Valero J. The role of CREB signaling in Alzheimer's disease and other cognitive disorders. *Reviews in the neurosciences.* 2011;22(2):153-69.
19. Wang A, and Bibb JA. Is CREB the angry bird that releases memory in Alzheimer's? *Neuropsychopharmacology : official publication of the American College of Neuropsychopharmacology.* 2011;36(11):2153-4.
20. Zhang L, Zambon AC, Vranizan K, Pothula K, Conklin BR, and Insel PA. Gene expression signatures of cAMP/protein kinase A (PKA)-promoted, mitochondrial-dependent apoptosis. Comparative analysis of wild-type and cAMP-deathless S49 lymphoma cells. *The Journal of biological chemistry.* 2008;283(7):4304-13.
21. Vitolo OV, Sant'Angelo A, Costanzo V, Battaglia F, Arancio O, and Shelanski M. Amyloid beta -peptide inhibition of the PKA/CREB pathway and long-term potentiation: reversibility by drugs that enhance cAMP signaling. *Proceedings of the National Academy of Sciences of the United States of America.* 2002;99(20):13217-21.
22. Espana J, Valero J, Minano-Molina AJ, Masgrau R, Martin E, Guardia-Laguarta C, et al. beta-Amyloid disrupts activity-dependent gene transcription required for memory through the CREB coactivator CRTC1. *The Journal of neuroscience : the official journal of the Society for Neuroscience.* 2010;30(28):9402-10.
23. Teich AF, Nicholls RE, Puzzo D, Fiorito J, Purgatorio R, Fa M, et al. Synaptic therapy in Alzheimer's disease: a CREB-centric approach. *Neurotherapeutics : the journal of the American Society for Experimental NeuroTherapeutics.* 2015;12(1):29-41.
24. Yiu AP, Rashid AJ, and Josselyn SA. Increasing CREB function in the CA1 region of dorsal hippocampus rescues the spatial memory deficits in a mouse model of Alzheimer's disease. *Neuropsychopharmacology : official publication of the American College of Neuropsychopharmacology.* 2011;36(11):2169-86.
25. Bartolotti N, Segura L, and Lazarov O. Diminished CRE-Induced Plasticity is Linked to Memory Deficits in Familial Alzheimer's Disease Mice. *Journal of Alzheimer's disease : JAD.* 2016;50(2):477-89.
26. Ettcheto M, Abad S, Petrov D, Pedrós I, Busquets O, Sánchez-López E, et al. Early Preclinical Changes in Hippocampal CREB-Binding Protein Expression in a Mouse Model of Familial Alzheimer’s Disease. *Molecular Neurobiology.* 2018;55(6):4885-95.
27. Dieterich DC, Karpova A, Mikhaylova M, Zdobnova I, Konig I, Landwehr M, et al. Caldendrin-Jacob: a protein liaison that couples NMDA receptor signalling to the nucleus. *PLoS biology.* 2008;6(2):e34.
28. Karpova A, Mikhaylova M, Bera S, Bär J, Reddy PP, Behnisch T, et al. Encoding and transducing the synaptic or extrasynaptic origin of NMDA receptor signals to the nucleus. *Cell.* 2013;152(5):1119-33.
29. Melgarejo da Rosa M, Yuanxiang P, Brambilla R, Kreutz MR, and Karpova A. Synaptic GluN2B/CaMKII-alpha Signaling Induces Synapto-Nuclear Transport of ERK and Jacob. *Frontiers in molecular neuroscience.* 2016;9:66.
30. Gomes GM, Dalmolin GD, Bär J, Karpova A, Mello CF, Kreutz MR, et al. Inhibition of the polyamine system counteracts beta-amyloid peptide-induced memory impairment in mice: involvement of extrasynaptic NMDA receptors. *PloS one.* 2014;9(6):e99184.

31. Grochowska KM, Yuanxiang P, Bär J, Raman R, Brugal G, Sahu G, et al. Posttranslational modification impact on the mechanism by which amyloid-beta induces synaptic dysfunction. *EMBO reports.* 2017;18(6):962-81.
32. Rönicke R, Mikhaylova M, Ronicke S, Meinhardt J, Schroder UH, Fandrich M, et al. Early neuronal dysfunction by amyloid beta oligomers depends on activation of NR2B-containing NMDA receptors. *Neurobiology of aging.* 2011;32(12):2219-28.
33. Kashani AH, Qiu Z, Jurata L, Lee SK, Pfaff S, Goebbels S, et al. Calcium activation of the LMO4 transcription complex and its role in the patterning of thalamocortical connections. *The Journal of neuroscience : the official journal of the Society for Neuroscience.* 2006;26(32):8398-408.
34. Joseph S, Kwan AH, Stokes PH, Mackay JP, Cubeddu L, and Matthews JM. The structure of an LIM-only protein 4 (LMO4) and Deformed epidermal autoregulatory factor-1 (DEAF1) complex reveals a common mode of binding to LMO4. *PloS one.* 2014;9(10):e109108-e.
35. Sala C, Rudolph-Correia S, and Sheng M. Developmentally regulated NMDA receptor-dependent dephosphorylation of cAMP response element-binding protein (CREB) in hippocampal neurons. *The Journal of neuroscience : the official journal of the Society for Neuroscience.* 2000;20(10):3529-36.
36. Huang KX, and Paudel HK. Ser67-phosphorylated inhibitor 1 is a potent protein phosphatase 1 inhibitor. *Proceedings of the National Academy of Sciences of the United States of America.* 2000;97(11):5824-9.
37. Jouvenceau A, Hedou G, Potier B, Kollen M, Dutar P, and Mansuy IM. Partial inhibition of PP1 alters bidirectional synaptic plasticity in the hippocampus. *The European journal of neuroscience.* 2006;24(2):564-72.
38. Morishita W, Connor JH, Xia H, Quinlan EM, Shenolikar S, and Malenka RC. Regulation of synaptic strength by protein phosphatase 1. *Neuron.* 2001;32(6):1133-48.
39. Oliver CJ, Terry-Lorenzo RT, Elliott E, Bloomer WA, Li S, Brautigan DL, et al. Targeting protein phosphatase 1 (PP1) to the actin cytoskeleton: the neurabin I/PP1 complex regulates cell morphology. *Molecular and cellular biology.* 2002;22(13):4690-701.
40. Song X, Jensen MO, Jogini V, Stein RA, Lee CH, McHaourab HS, et al. Mechanism of NMDA receptor channel block by MK-801 and memantine. *Nature.* 2018;556(7702):515-9.
41. Kummer MP, and Heneka MT. Truncated and modified amyloid-beta species. *Alzheimer's research & therapy.* 2014;6(3):28.
42. Bayer TA, and Wirths O. Focusing the amyloid cascade hypothesis on N-truncated Abeta peptides as drug targets against Alzheimer's disease. *Acta neuropathologica.* 2014;127(6):787-801.
43. Jawhar S, Wirths O, and Bayer TA. Pyroglutamate amyloid-β (Aβ): a hatchet man in Alzheimer disease. *The Journal of biological chemistry.* 2011;286(45):38825-32.
44. Perez-Garmendia R, and Gevorkian G. Pyroglutamate-Modified Amyloid Beta Peptides: Emerging Targets for Alzheimer´s Disease Immunotherapy. *Curr Neuropharmacol.* 2013;11(5):491-8.
45. Morawski M, Schilling S, Kreuzberger M, Waniek A, Jäger C, Koch B, et al. Glutaminyl cyclase in human cortex: correlation with (pGlu)-amyloid-β load and cognitive decline in Alzheimer's disease. *Journal of Alzheimer's disease : JAD.* 2014;39(2):385-400.

46. Hartlage-Rübsamen M, Morawski M, Waniek A, Jäger C, Zeitschel U, Koch B, et al. Glutaminyl cyclase contributes to the formation of focal and diffuse pyroglutamate (pGlu)-Aβ deposits in hippocampus via distinct cellular mechanisms. *Acta neuropathologica.* 2011;121(6):705-19.
47. Schilling S, Zeitschel U, Hoffmann T, Heiser U, Francke M, Kehlen A, et al. Glutaminyl cyclase inhibition attenuates pyroglutamate Abeta and Alzheimer's disease-like pathology. *Nature medicine.* 2008;14(10):1106-11.
48. Alexandru A, Jagla W, Graubner S, Becker A, Bäuscher C, Kohlmann S, et al. Selective hippocampal neurodegeneration in transgenic mice expressing small amounts of truncated Aβ is induced by pyroglutamate-Aβ formation. *The Journal of neuroscience : the official journal of the Society for Neuroscience.* 2011;31(36):12790-801.
49. Padurariu M, Ciobica A, Mavroudis I, Fotiou D, and Baloyannis S. Hippocampal neuronal loss in the CA1 and CA3 areas of Alzheimer's disease patients. *Psychiatria Danubina.* 2012;24(2):152-8.
50. Masurkar AV. Towards a circuit-level understanding of hippocampal CA1 dysfunction in Alzheimer's disease across anatomical axes. *Journal of Alzheimer's disease & Parkinsonism.* 2018;8(1).
51. Hyman BT, Van Hoesen GW, Damasio AR, and Barnes CL. Alzheimer's disease: cell-specific pathology isolates the hippocampal formation. *Science.* 1984;225(4667):1168-70.
52. Ingelsson M, Fukumoto H, Newell KL, Growdon JH, Hedley-Whyte ET, Frosch MP, et al. Early Abeta accumulation and progressive synaptic loss, gliosis, and tangle formation in AD brain. *Neurology.* 2004;62(6):925-31.
53. Braak H, and Braak E. Neuropathological stageing of Alzheimer-related changes. *Acta neuropathologica.* 1991;82(4):239-59.
54. Serrano-Pozo A, Frosch MP, Masliah E, and Hyman BT. Neuropathological alterations in Alzheimer disease. *Cold Spring Harbor perspectives in medicine.* 2011;1(1):a006189.
55. Mikhaylova M, Karpova A, Bär J, Bethge P, YuanXiang P, Chen Y, et al. Cellular distribution of the NMDA-receptor activated synapto-nuclear messenger Jacob in the rat brain. *Brain structure & function.* 2014;219(3):843-60.
56. Bartolotti N, Bennett DA, and Lazarov O. Reduced pCREB in Alzheimer's disease prefrontal cortex is reflected in peripheral blood mononuclear cells. *Molecular psychiatry.* 2016;21(9):1158-66.
57. Yamamoto-Sasaki M, Ozawa H, Saito T, Rosler M, and Riederer P. Impaired phosphorylation of cyclic AMP response element binding protein in the hippocampus of dementia of the Alzheimer type. *Brain research.* 1999;824(2):300-3.
58. Pugazhenthi S, Wang M, Pham S, Sze CI, and Eckman CB. Downregulation of CREB expression in Alzheimer's brain and in Abeta-treated rat hippocampal neurons. *Molecular neurodegeneration.* 2011;6:60.
59. Parra-Damas A, Chen M, Enriquez-Barreto L, Ortega L, Acosta S, Perna JC, et al. CRTC1 Function During Memory Encoding Is Disrupted in Neurodegeneration. *Biological psychiatry.* 2017;81(2):111-23.
60. Francis YI, Stephanou A, and Latchman DS. CREB-binding protein activation by presenilin 1 but not by its M146L mutant. *Neuroreport.* 2006;17(9):917-21.

61. Parra-Damas A, and Saura CA. Synapse-to-Nucleus Signaling in Neurodegenerative and Neuropsychiatric Disorders. *Biological psychiatry.* 2019;86(2):87-96.
62. Chen HH, Xu J, Safarpour F, and Stewart AF. LMO4 mRNA stability is regulated by extracellular ATP in F11 cells. *Biochemical and biophysical research communications.* 2007;357(1):56-61.
63. Schock SC, Xu J, Duquette PM, Qin Z, Lewandowski AJ, Rai PS, et al. Rescue of neurons from ischemic injury by peroxisome proliferator-activated receptor-gamma requires a novel essential cofactor LMO4. *The Journal of neuroscience : the official journal of the Society for Neuroscience.* 2008;28(47):12433-44.
64. Hahm K, Sum EY, Fujiwara Y, Lindeman GJ, Visvader JE, and Orkin SH. Defective neural tube closure and anteroposterior patterning in mice lacking the LIM protein LMO4 or its interacting partner Deaf-1. *Molecular and cellular biology.* 2004;24(5):2074-82.
65. Manetopoulos C, Hansson A, Karlsson J, Jonsson JI, and Axelson H. The LIM-only protein LMO4 modulates the transcriptional activity of HEN1. *Biochemical and biophysical research communications.* 2003;307(4):891-9.
66. Sum EY, Peng B, Yu X, Chen J, Byrne J, Lindeman GJ, et al. The LIM domain protein LMO4 interacts with the cofactor CtIP and the tumor suppressor BRCA1 and inhibits BRCA1 activity. *The Journal of biological chemistry.* 2002;277(10):7849-56.
67. Singh RR, Barnes CJ, Talukder AH, Fuqua SA, and Kumar R. Negative regulation of estrogen receptor alpha transactivation functions by LIM domain only 4 protein. *Cancer research.* 2005;65(22):10594-601.
68. Zhou X, Sang M, Liu W, Gao W, Xing E, Lu W, et al. LMO4 inhibits p53-mediated proliferative inhibition of breast cancer cells through interacting p53. *Life sciences.* 2012;91(9-10):358-63.
69. Asprer JS, Lee B, Wu CS, Vadakkan T, Dickinson ME, Lu HC, et al. LMO4 functions as a co-activator of neurogenin 2 in the developing cortex. *Development (Cambridge, England).* 2011;138(13):2823-32.
70. Strack S, Kini S, Ebner FF, Wadzinski BE, and Colbran RJ. Differential cellular and subcellular localization of protein phosphatase 1 isoforms in brain. *The Journal of comparative neurology.* 1999;413(3):373-84.
71. Bito H, Deisseroth K, and Tsien RW. CREB phosphorylation and dephosphorylation: a Ca(2+)- and stimulus duration-dependent switch for hippocampal gene expression. *Cell.* 1996;87(7):1203-14.
72. Cohen PT. Protein phosphatase 1--targeted in many directions. *Journal of cell science.* 2002;115(Pt 2):241-56.
73. Bollen M, Peti W, Ragusa MJ, and Beullens M. The extended PP1 toolkit: designed to create specificity. *Trends in biochemical sciences.* 2010;35(8):450-8.
74. Peti W, Nairn AC, and Page R. Structural basis for protein phosphatase 1 regulation and specificity. *FEBS J.* 2013;280(2):596-611.
75. Braak H, and Braak E. Staging of Alzheimer's disease-related neurofibrillary changes. *Neurobiology of aging.* 1995;16(3):271-8; discussion 8-84.
76. Smith DL, Pozueta J, Gong B, Arancio O, and Shelanski M. Reversal of long-term dendritic spine alterations in Alzheimer disease models. *Proceedings of the National Academy of Sciences of the United States of America.* 2009;106(39):16877-82.

77. Gong B, Vitolo OV, Trinchese F, Liu S, Shelanski M, and Arancio O. Persistent improvement in synaptic and cognitive functions in an Alzheimer mouse model after rolipram treatment. *The Journal of clinical investigation.* 2004;114(11):1624-34.
78. Sierksma AS, van den Hove DL, Pfau F, Philippens M, Bruno O, Fedele E, et al. Improvement of spatial memory function in APPswe/PS1dE9 mice after chronic inhibition of phosphodiesterase type 4D. *Neuropharmacology.* 2014;77:120-30.
79. Coleman PD, and Yao PJ. Synaptic slaughter in Alzheimer's disease. *Neurobiology of aging.* 2003;24(8):1023-7.
80. Xia P, Chen HS, Zhang D, and Lipton SA. Memantine preferentially blocks extrasynaptic over synaptic NMDA receptor currents in hippocampal autapses. *The Journal of neuroscience : the official journal of the Society for Neuroscience.* 2010;30(33):11246-50.
81. Reisberg B, Doody R, Stoffler A, Schmitt F, Ferris S, and Mobius HJ. Memantine in moderate-to-severe Alzheimer's disease. *The New England journal of medicine.* 2003;348(14):1333-41.
82. Wang X, Blanchard J, Grundke-Iqbal I, and Iqbal K. Memantine Attenuates Alzheimer's Disease-Like Pathology and Cognitive Impairment. *PloS one.* 2015;10(12):e0145441.
83. Spilker C, Nullmeier S, Grochowska KM, Schumacher A, Butnaru I, Macharadze T, et al. A Jacob/Nsmf Gene Knockout Results in Hippocampal Dysplasia and Impaired BDNF Signaling in Dendritogenesis. *PLoS Genet.* 2016;12(3):e1005907-e.
84. Mirra SS, Heyman A, McKeel D, Sumi SM, Crain BJ, Brownlee LM, et al. The Consortium to Establish a Registry for Alzheimer's Disease (CERAD). Part II. Standardization of the neuropathologic assessment of Alzheimer's disease. *Neurology.* 1991;41(4):479-86.
85. Trinkle-Mulcahy L, Sleeman JE, and Lamond AI. Dynamic targeting of protein phosphatase 1 within the nuclei of living mammalian cells. *Journal of cell science.* 2001;114(Pt 23):4219-28.
86. Liu D, Vleugel M, Backer CB, Hori T, Fukagawa T, Cheeseman IM, et al. Regulated targeting of protein phosphatase 1 to the outer kinetochore by KNL1 opposes Aurora B kinase. *J Cell Biol.* 2010;188(6):809-20.
87. Helmuth M, Altrock W, Böckers TM, Gundelfinger ED, and Kreutz MR. An electrotransfection protocol for yeast two-hybrid library screening. *Anal Biochem.* 2001;293(1):149-52.
88. Carriba P, Navarro G, Ciruela F, Ferre S, Casado V, Agnati L, et al. Detection of heteromerization of more than two proteins by sequential BRET-FRET. *Nature methods.* 2008;5(8):727-33.
89. Mikhaylova M, Reddy PP, Munsch T, Landgraf P, Suman SK, Smalla K-H, et al. Calneurons provide a calcium threshold for trans-Golgi network to plasma membrane trafficking. *Proceedings of the National Academy of Sciences of the United States of America.* 2009;106(22):9093-8.
90. Schindelin J, Arganda-Carreras I, Frise E, Kaynig V, Longair M, Pietzsch T, et al. Fiji: an open-source platform for biological-image analysis. *Nature methods.* 2012;9(7):676-82.
91. Nussbaum JM, Schilling S, Cynis H, Silva A, Swanson E, Wangsanut T, et al. Prion-like behaviour and tau-dependent cytotoxicity of pyroglutamylated amyloid-β. *Nature.* 2012;485(7400):651-5.

92. Kapitein LC, van Bergeijk P, Lipka J, Keijzer N, Wulf PS, Katrukha EA, et al. Myosin-V opposes microtubule-based cargo transport and drives directional motility on cortical actin. *Curr Biol.* 2013;23(9):828-34.
93. Gee CE, Ohmert I, Wiegert JS, and Oertner TG. Preparation of Slice Cultures from Rodent Hippocampus. *Cold Spring Harb Protoc.* 2017;2017(2):10.1101/pdb.prot094888.

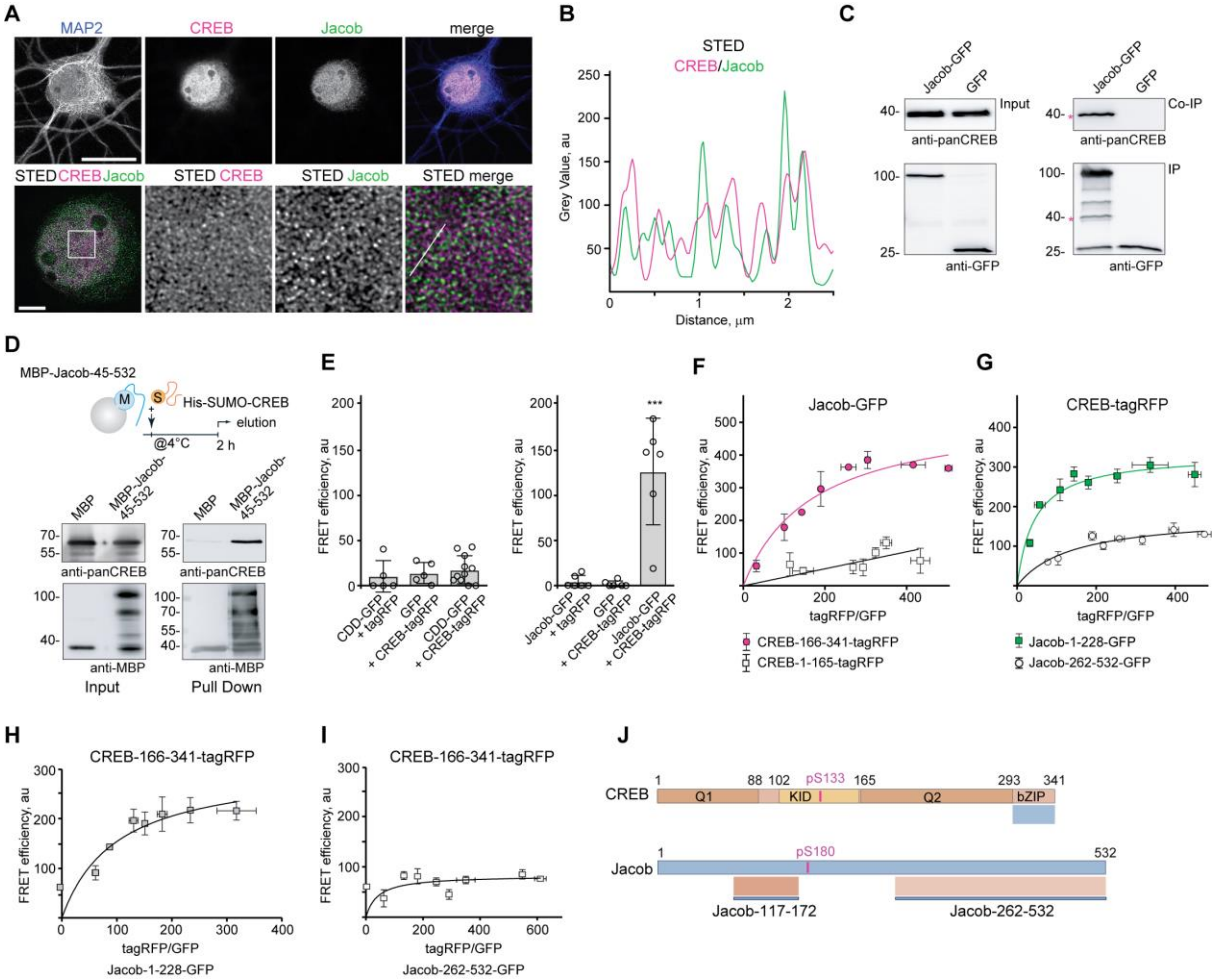

Figure 1. Nuclear Jacob directly associates with CREB.

A, B) Confocal and STED images show an association of CREB with Jacob in the nucleus of DIV16 hippocampal primary neurons stained with antibodies directed against pan-CREB, pan-Jacob, and MAP2. (A) The upper panel represents deconvolved confocal images. Lower panels depict deconvolved STED images. Scale bars: 20 µm and 5 µm respectively. Inserts are denoted by a white square. (B) Line profiles indicate the overlap of relative intensities for CREB and Jacob along a 2.5 µm line depicted in white in the merged image.

C) Endogenous CREB co-immunoprecipitates with overexpressed Jacob-GFP, but not GFP from HEK293T cell extracts. The asterisk denotes the CREB band from a membrane subsequently re-probed with an anti-GFP antibody.

D) Pull-down assay confirms a direct interaction of MBP-Jacob-45-532 and His-SUMO-CREB.

E) FRET measurements performed in HEK293T cells show significant FRET between CREB-tagRFP and Jacob-GFP but not between controls (tagRFP or Caldendrin (CDD-GFP). Bar plot representing mean values of 5 independent experiments measured in triplicates ± SEM. ***p<0,001 by one-way ANOVA followed by Bonferroni's multiple comparisons test.

F) The C-terminus but not the N-terminus of CREB closely associates with Jacob-GFP in FRET saturation experiments.

G) FRET saturation experiments in cells transfected with CREB-tagRFP and Jacob-1-228-GFP or Jacob-262-532-GFP revealed that both N- and C-termini of Jacob are

in close proximity to CREB, however the Jacob-1-228-GFP association with CREB is significantly stronger.
H, I) The C-terminus of CREB associates with both N- and C-termini of Jacob. However, association with Jacob-1-228-GFP is much stronger compared to its C-terminus (Jacob-262-532-GFP).
(F-I) FRET saturation experiments were performed in the HEK293T cell suspension. FRET efficiency is given in arbitrary units as a means of 5-6 independent experiments. Data are represented as mean ± SEM.
J) Scheme depicting domain organization and binding interfaces. Jacob binds to the bZIP domain of CREB (blue box). The orange box indicates a stronger interaction of the Jacob N-terminus, the shaded orange box indicates a weaker association of the C-terminus.

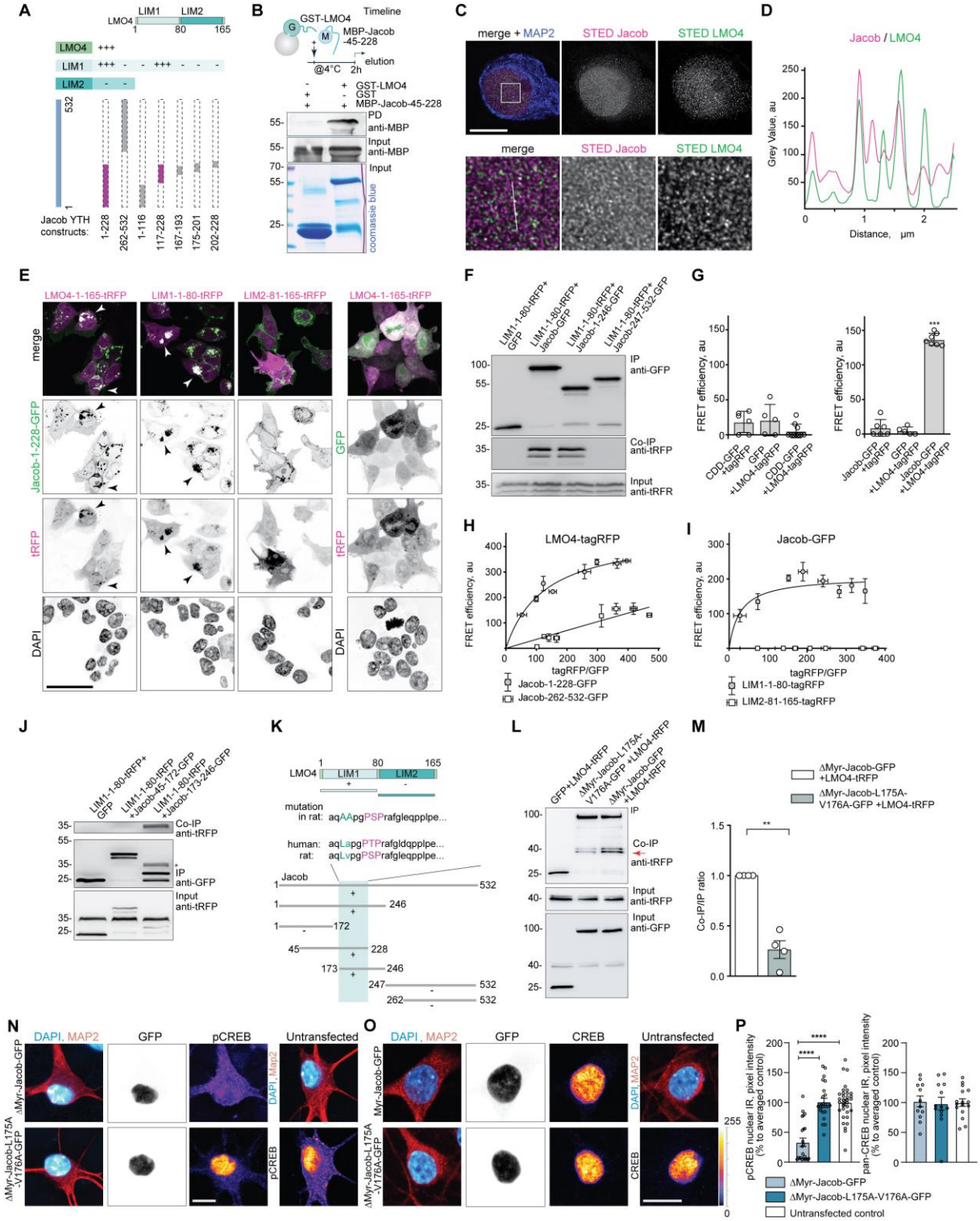

Figure 2. LMO4 is a direct binding partner of Jacob.

A) Jacob-117-228 interacts with the LIM1 domain of LMO4 in Y2H. (+++) indicates a strong interaction while (–) indicates no interaction. Evaluation was based on the number of colonies growing in triple drop-out media.

B) The GST-LMO4 fusion protein but not control GST pulls down recombinant MBP-Jacob-45-228.

C, D) Super-resolution STED imaging revealed association of Jacob with LMO4 in the nucleus (C). DIV16 primary hippocampal neurons stained with antibodies against

MAP2, LMO4, pan-Jacob. Upper panel - scale bar:10 µm, lower panel (inserts 5 µm x 5 µm – denoted by the white square). (D) Line profiles indicate relative intensities for deconvolved STED channels along a 2.5 µm line (depicted in white).

E) Jacob-1-228-GFP co-recruits the LIM1 (1-80), but not LIM2 (81-165) domain of LMO4. Confocal images of HEK293T cells transfected either with Jacob-1-228-GFP or GFP as a control and different fragments of LMO4. Arrows indicate co-recruitment. Scale bar is 40 µm.

F) LIM1-1-80-tRFP co-immunoprecipitates with Jacob-1-246-GFP, but not Jacob-247-532-GFP from HEK293T cell extracts.

G) FRET experiments in transfected HEK293T cells suspensions showing that Jacob-GFP, but not CDD-GFP or GFP alone, interacts with LMO4-tagRFP. Bar plot representing mean values of 6 independent experiments measured in triplicates ± SEM. ***p<0,001 by one-way ANOVA followed by Bonferroni's multiple comparisons test.

H, I) FRET saturation experiments indicating the association of Jacob-1-228-GFP with LIM-1-80-tagRFP. FRET efficiency is given in arbitrary units as a mean of 6 independent experiments. Data represented as mean ± SEM.

J) Further mapping for Jacob binding to the LIM1 domain of LMO4 reviled its association with 179-246 aa of Jacob, but not with Jacob-45-172-GFP (CREB-binding region).

K) Scheme summarizing LMO4-Jacob interaction regions, crucial residues within the region among species and mutated amino acids within the rat sequence (L175A, V176A).

L, M) Leucine at position 175 is crucial for the association of Jacob with LMO4. Heterologous co-immunoprecipitation experiments between LMO4-tagRFP and nuclear ΔMyr-Jacob-GFP, ΔMyr-Jacob-L175A-V176A-GFP or GFP overexpressed in HEK293T cells revealed decreased association of ΔMyr-Jacob-L175A-V176A-GFP with LMO4 compare to ΔMyr-Jacob-GFP. **p<0,01 by one-sample t-test from 4 independent experiments

N-P) A Jacob-LMO4-binding mutant expressed in the nucleus does not induce CREB shut-off. (N, O) Representative confocal images of hippocampal neurons transfected with ΔMyr-Jacob-GFP or ΔMyr-Jacob-L175A-V176A-GFP. Scale bar: 10 µm. (P) Dot plots representing mean of nuclear pCREB immunoreactivity in Jacob-expressing neurons normalized to untransfected control. "N" corresponds to the number of neuronal nuclei analyzed from two independent cell cultures. Data are represented as mean ± SEM. ****p<0,0001 by one-way ANOVA followed by Tukey's multiple comparisons test.

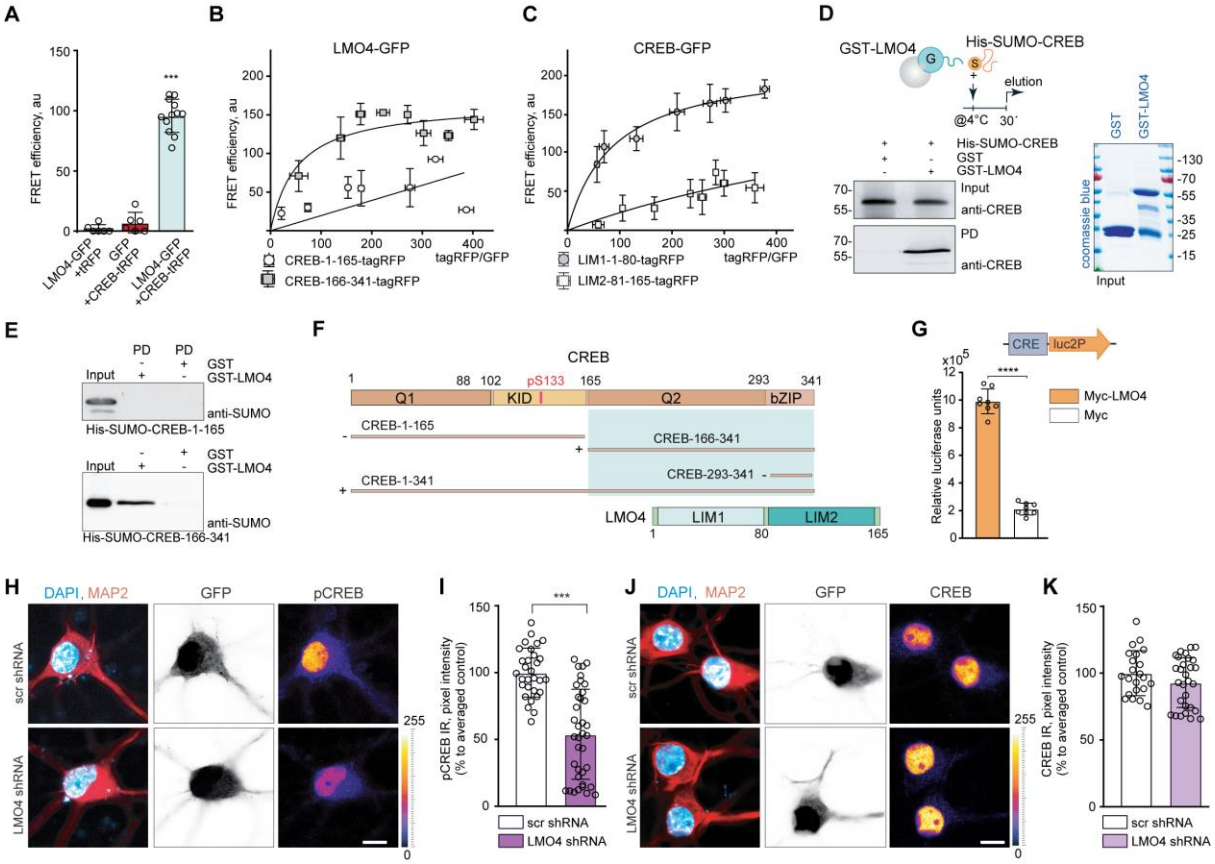

Figure 3. LMO4 is an interaction partner of CREB.

A) FRET measurements indicate a tight association between LMO4-GFP and CREB-tagRFP expressed in HEK293T cells. Bar plot representing mean values of 6 independent experiments measured in triplicates ± SEM, ***p<0,001 by one-way ANOVA followed by Bonferroni's multiple comparisons test.

B, C) FRET saturation experiments with (B) LMO4-GFP and CREB-1-165-tagRFP or (C) CREB-166-341-tagRFP and CREB-GFP and LIM1-1-80-tagRFP or LIM2-81-165-tagRFP revealed the association between LIM1 domain of LMO4 and C-terminus of CREB. Box plots of FRET arbitrary units from 8 independent experiments. Data represented as mean ± SEM.

D) Bacterially produced recombinant His-SUMO-CREB directly binds to GST-LMO4 in pull-down experiments. Cartoon represents the scheme of the experiment.

E) The interaction between CREB with LMO4 is mediated by the C-terminus of CREB (166-341 aa), but not by its N-terminus (1-165 aa). Pull-down experiments between bacterially produced His-SUMO-1-165-CREB, His-SUMO-166-341-CREB and GST-LMO4.

F) Schematic representation of CREB and LMO4 domain structure and fusion constructs used for the experiments. Light green boxes represent the interaction interface.

G) Myc-LMO4 overexpression increases CREB dependent luciferase expression in HEK293T cells stably transfected with pGL4.29 [luc2P/CRE/Hygro] vector expressing luciferase under the CRE promoter. Depicted are the relative luciferase units in cells overexpressing Myc-LMO4 as compared to Myc-transfected controls. N=8, from two independent experiments. Data are represented as mean ± SEM. ****p<0,0001 by two-tailed Student t-test.

H - K) Knockdown of LMO4 reduces nuclear pCREB immunoreactivity. (H, J) Representative confocal images of hippocampal neurons transfected with LMO4 shRNA construct or scrambled control (both expressing GFP under CMV promoter as a transfection control). Scale bar: 10µm. Dot plots representing the mean of nuclear (I) pCREB or (K) CREB staining intensity normalized to scrambled control. “N” corresponds to the number of nuclei analyzed from at least 3 independent cell cultures. Data are represented as mean ± SEM. ***p<0,001 by two-tailed Student’s t-test.

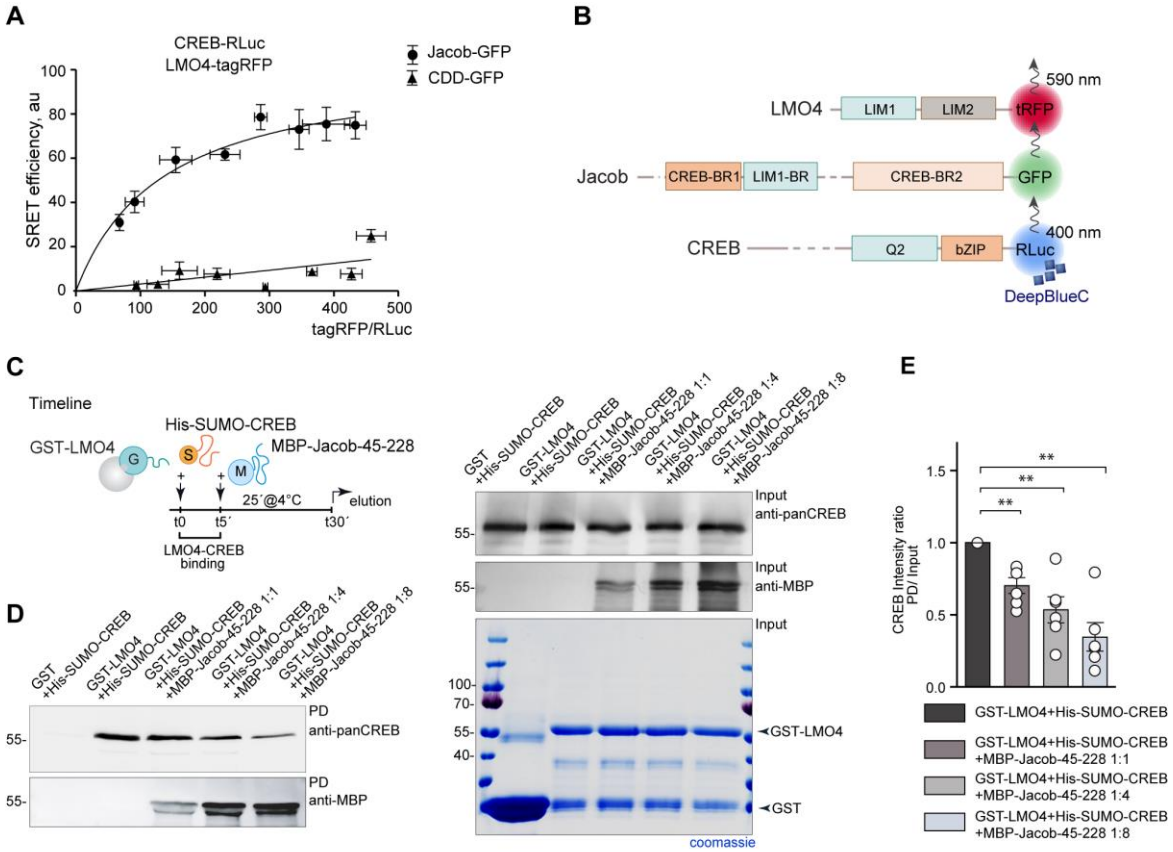

Figure 4. Jacob displaces LMO4 from CREB.

A, B) SRET saturation experiments reveal that Jacob-GFP can form a triple complex with CREB-RLuc and LMO4-tagRFP. HEK293T cells were transfected with CREB-RLuc and LMO4-tagRFP and (A) Jacob-GFP or CDD-GFP (negative control). Data represented as mean ± SEM of 8 independent experiments. SRET saturation curve indicates binding between respective proteins while straight line represents no interaction. (B) Schematic representation of constructs used in SRET experiments. “BR” stands for binding region.

C, D, E) The N-terminus of Jacob displaces LMO4 from CREB. Schematic depicts the timeline of the competition pull-down experiment where GST-LMO4 coupled to beads was preincubated with His-SUMO-CREB and subsequently incubated with an enhanced amount of MBP-Jacob-45-228 (C). Immunoblot developed with anti-CREB and anti-MBP antibodies showing decreased intensity for the CREB band upon increasing concentration of MBP-Jacob-45-228. (D) The image of a coomassie blue stained gel represents GST-LMO4 and GST control coupled to beads. (E) Quantification of CREB band intensity normalized to the input (n=6). Data represented as mean ± SEM. **p<0,01 by one-sample t-test.

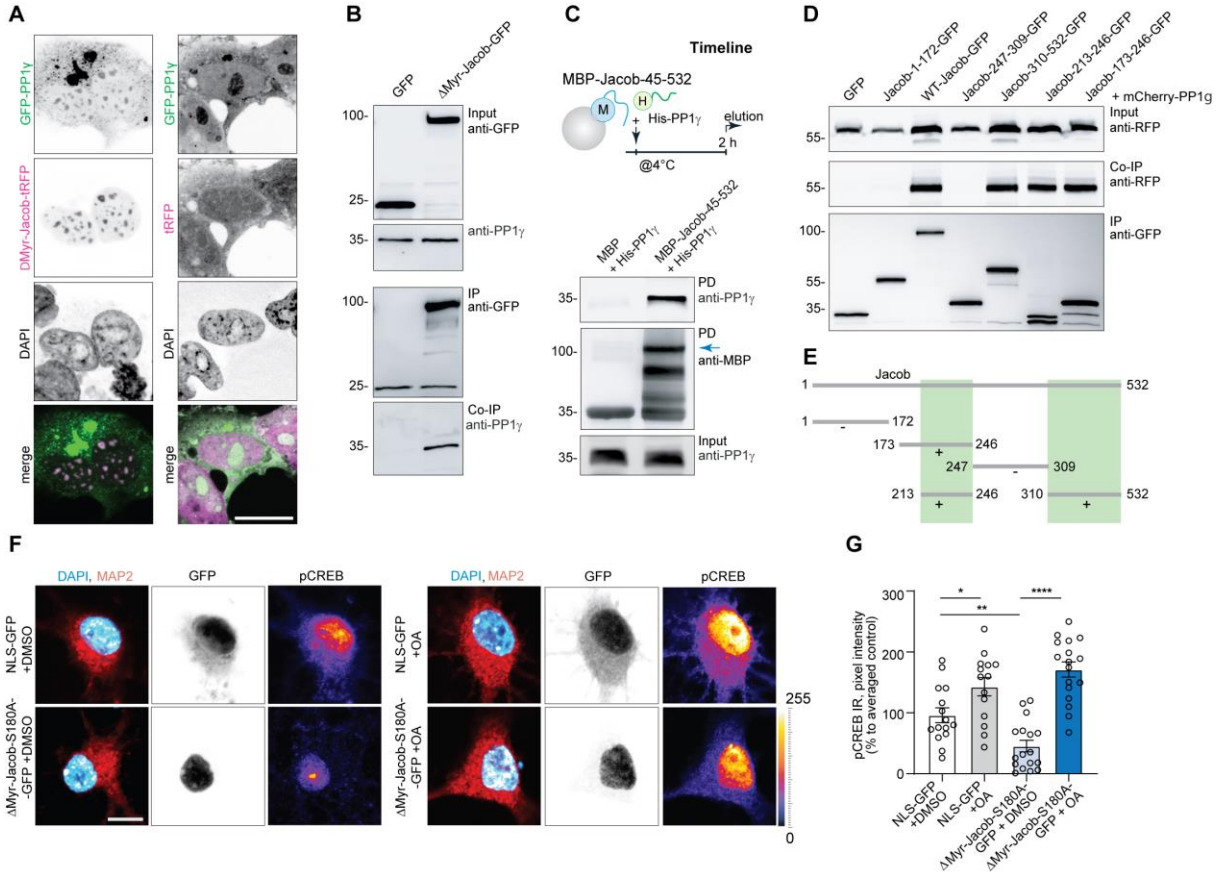

Figure 5. Jacob binds PP1 and association with PP1 is crucial for the CREB shut-off.

A) Confocal images of HEK293T cells overexpressing GFP-PP1γ together with ether ΔMyr-Jacob-tagRFP or tRFP control revealed nuclear co-clustering of both proteins. Scale bar: 20 µm.
B) ΔMyr-Jacob-GFP but not GFP co-immunoprecipitate with endogenous PP1γ from HEK293T cells extracts.
C) Pull-down experiments confirmed a direct interaction between bacterially produced recombinant MBP-Jacob-45-532 and His-PP1γ.
D, E) Mapping of the PP1γ interaction region within the Jacob sequence revealed binding of a C-terminal fragment (Jacob-310-250-GFP) as well as the N-terminal part (Jacob-173-246-GFP) where the region between 213-246 aa is sufficient for immunoprecipitation. Immunoblot represents heterologous Co-IP from HEK293T cells transfected with mCherry-PP1γ and different fragments of Jacob fused with GFP or GFP alone. (E) The scheme represents the different Jacob fragments used for CoIP. Green boxes indicate interaction regions.
F, G) Treatment of hippocampal primary neurons expressing phosphodeficient mutant Jacob in the nucleus with okadaic acid rescues Jacob-induced CREB shut-off. Confocal images of pCREB immunostaining in DIV15 neurons overexpressing ΔMyr-Jacob-S180A-GFP with and without OA treatment. Scale bar: 20 µm. "N" corresponds to the number of nuclei analyzed from 2 independent cell cultures. Data represented as mean ± SEM. ****p<0,0001 vs. non-transfected control by repeated measures two-way ANOVA followed by two-tailed Student's t-test.

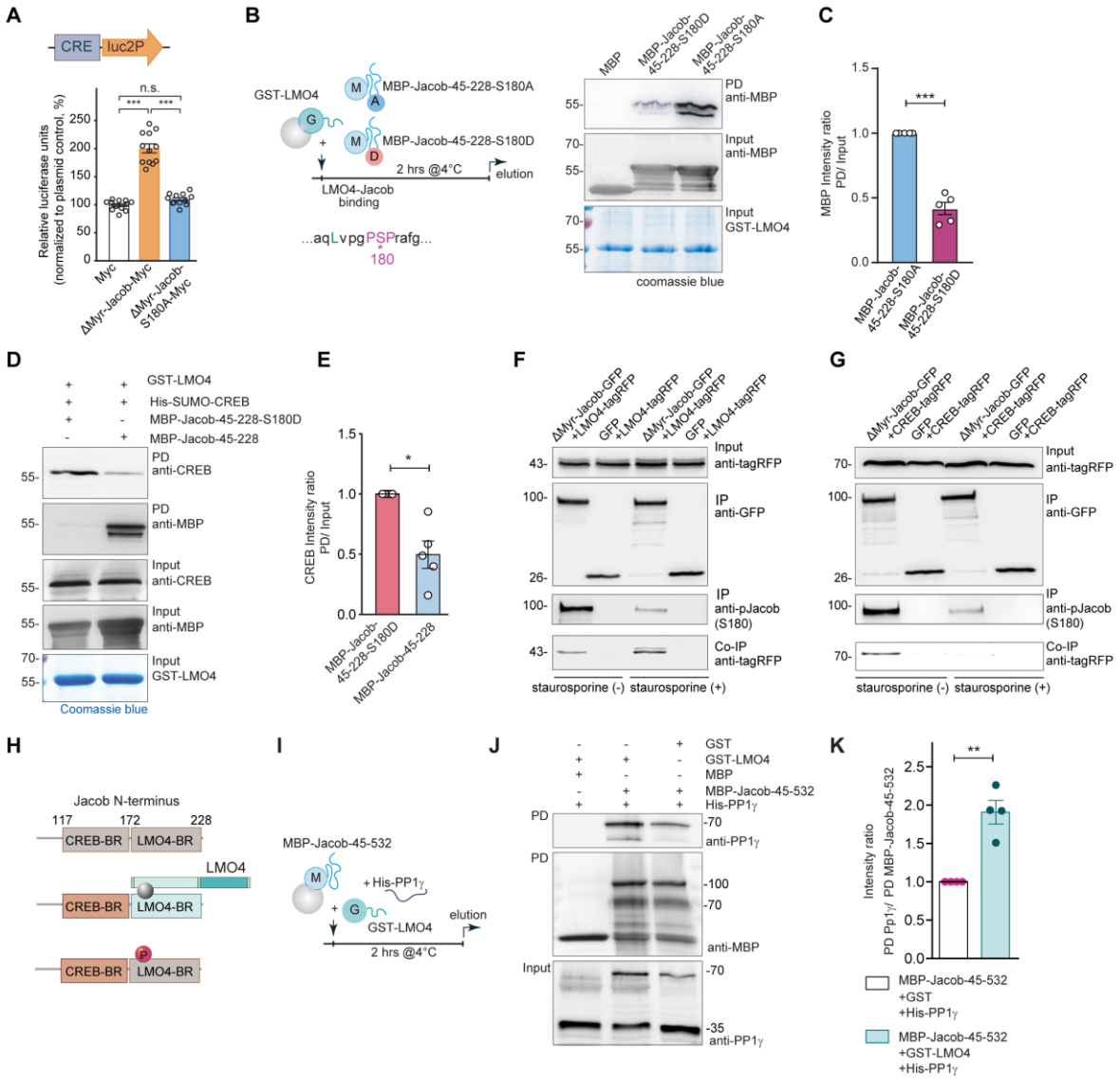

Figure 6. Interaction of Jacob with LMO4 critically depends on phosphorylation at Ser180.

A) Overexpression of ΔMyr-Jacob-Myc but not the phospho-deficient mutant (ΔMyr-Jacob-S180A-Myc) positively regulates CREB dependent expression of luciferase measured as luciferase activity in a stably transfected HEK293T cell line (pGL4.29[luc2P/CRE/Hygro] Vector). Data are represented as mean ± SEM from 3 independent experiments. ***p<0,001 by one-way ANOVA followed by Bonferroni's multiple comparisons test.

B, C) Phosphodeficient N-terminus of Jacob (MBP-Jacob-45-228-180A) interacts with LMO4 stronger than its phosphomimetic form (MBP-Jacob-45-228-180D). The scheme depicts the experimental outline, where bacterially expressed GST-LMO4 immobilized on beads was incubated with either MBP-Jacob-45-228-180A or MBP-Jacob-45-228-180D. (C) Bar graph represents quantification of MBP immunoreactivity normalized to input. N=5, ***p<0,001 by one-sample t-test.

D-E) Phosphomimetic Jacob mutant (MBP-45-228-180D) is unable to displace LMO4 from CREB. Recombinant GST-LMO4 was coupled to beads, preincubated with His-SUMO-CREB and subsequently incubated in 1:8 ratio with MBP-Jacob-45-228 or MBP-45-228-180D. Immunoblot developed with anti-CREB antibody. The image of

coomassie blue stained gel represents the GST-LMO4 input. (E) Quantification of the CREB band intensity normalized to the input. N=5. Data represented as mean ± SEM. *p<0,05 by one-sample t-test.

F) Treatment with staurosporine decreases Jacob phosphorylation level (S180), but increases its association with LMO4-tagRFP. Immunoblot of HEK293T cells extracts transfected with LMO4-tagRFP and ΔMyr-Jacob-GFP or GFP alone.

G) Treatment with staurosporine decreases the association of Jacob with CREB. Immunoblot of HEK293T cells extract transfected with CREB-tagRFP and ΔMyr-Jacob-GFP or GFP as a control.

H) Scheme summarizing the phosphorylation-dependent association of the N-terminus of Jacob with LMO4.

I-K) The association of Jacob with LMO4 enhance its interaction with PP1γ in pull-down assays. (J) PP1γ interacts with Jacob as a dimer (70 kDa) that forms during purification. (K) Bar graph represents quantification of PP1γ immunoreactivity normalized to MBP-Jacob. N=4, **p<0,01 by one-sample t-test.

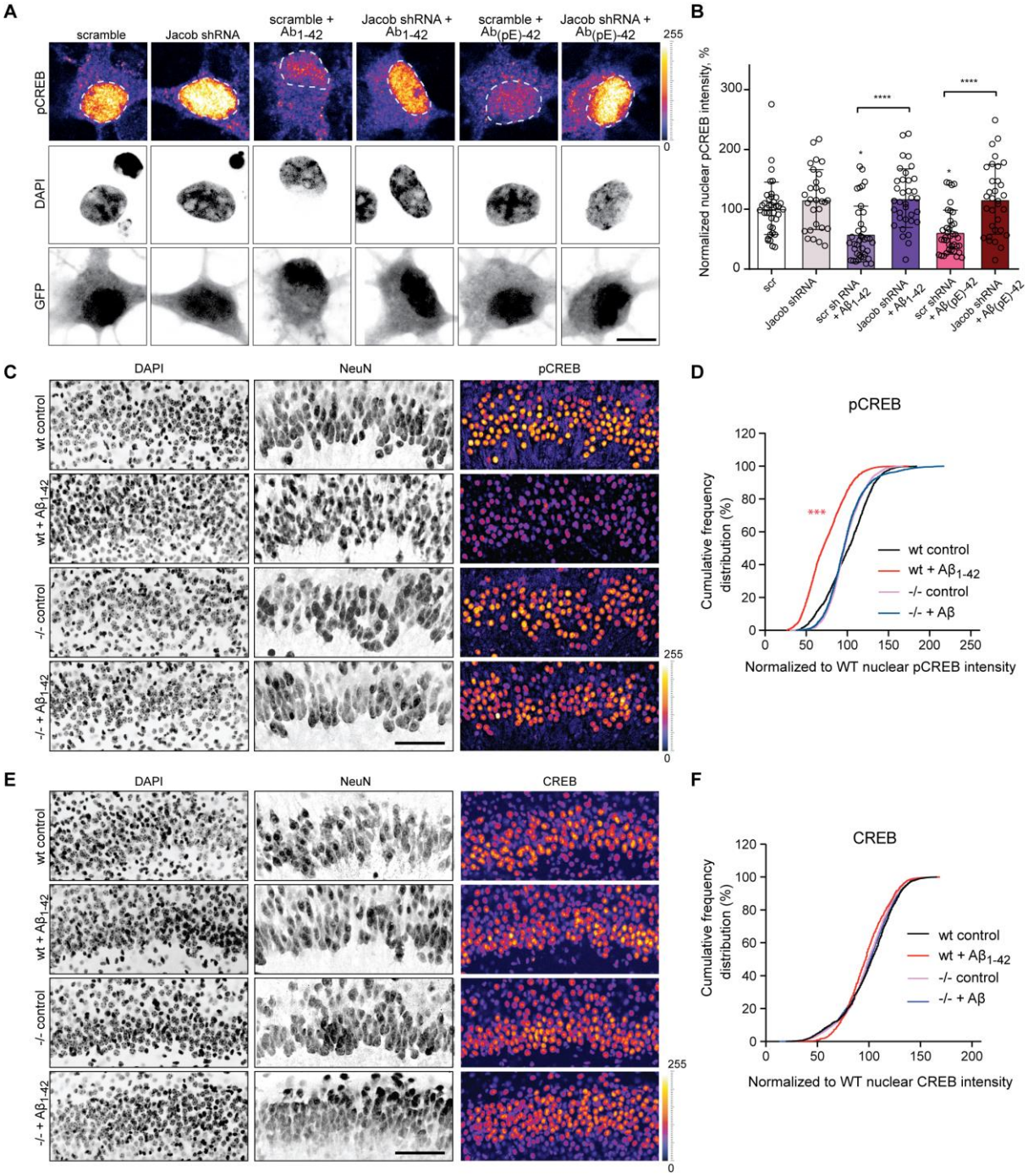

Figure 7. Jacob mediates Aβ-induced CREB shut-off

A, B) Jacob shRNA knockdown prevents Aβ-induced CREB shut-off. Representative confocal images of hippocampal neurons transfected with Jacob-shRNA construct or scrambled (scr) shRNA control (both expressing GFP) and treated with oligomeric preparations of $A\beta_{1-42}$ or $A\beta_{3(pE)-42}$. (B) Contrary to the scr shRNA, neurons transfected with Jacob knockdown construct did not display reduction of pCREB staining intensity after treatment with $A\beta_{1-42}$ or $A\beta_{3(pE)-42}$. Bar plot of mean nuclear pCREB intensity normalized to scramble untreated control. Scale bar: 10 µm. N=29-39 nuclei from 2 independent experiments. ****p<0,0001 by 2way ANOVA followed by Sidak's multiple comparisons test, *p<0,05 by two-way ANOVA followed by Tukey's multiple comparisons test. Data are represented as mean ± SEM. Lookup table indicates the pixel intensities from 0 to 255.

C-F) Acute (1h) $A\beta_{1-42}$ treatment does not induce CREB shut-off in organotypic hippocampal slices from Jacob knock-out mice. Representative confocal images of slices immunolabeled against pCREB (C) or panCREB (E), co-labeled with anti-NeuN antibody and co-stained with DAPI. Cumulative frequency distribution of pCREB (D) and panCREB (F) nuclear staining intensity. (D) N=2320-3669 nuclei from 16-22 slices. (F) N=1177-2079 nuclei from 11-14 slices. ***p<0,001 by two-way ANOVA followed by Tukey's multiple comparisons test. Lookup table indicates the pixel intensities from 0 to 255.

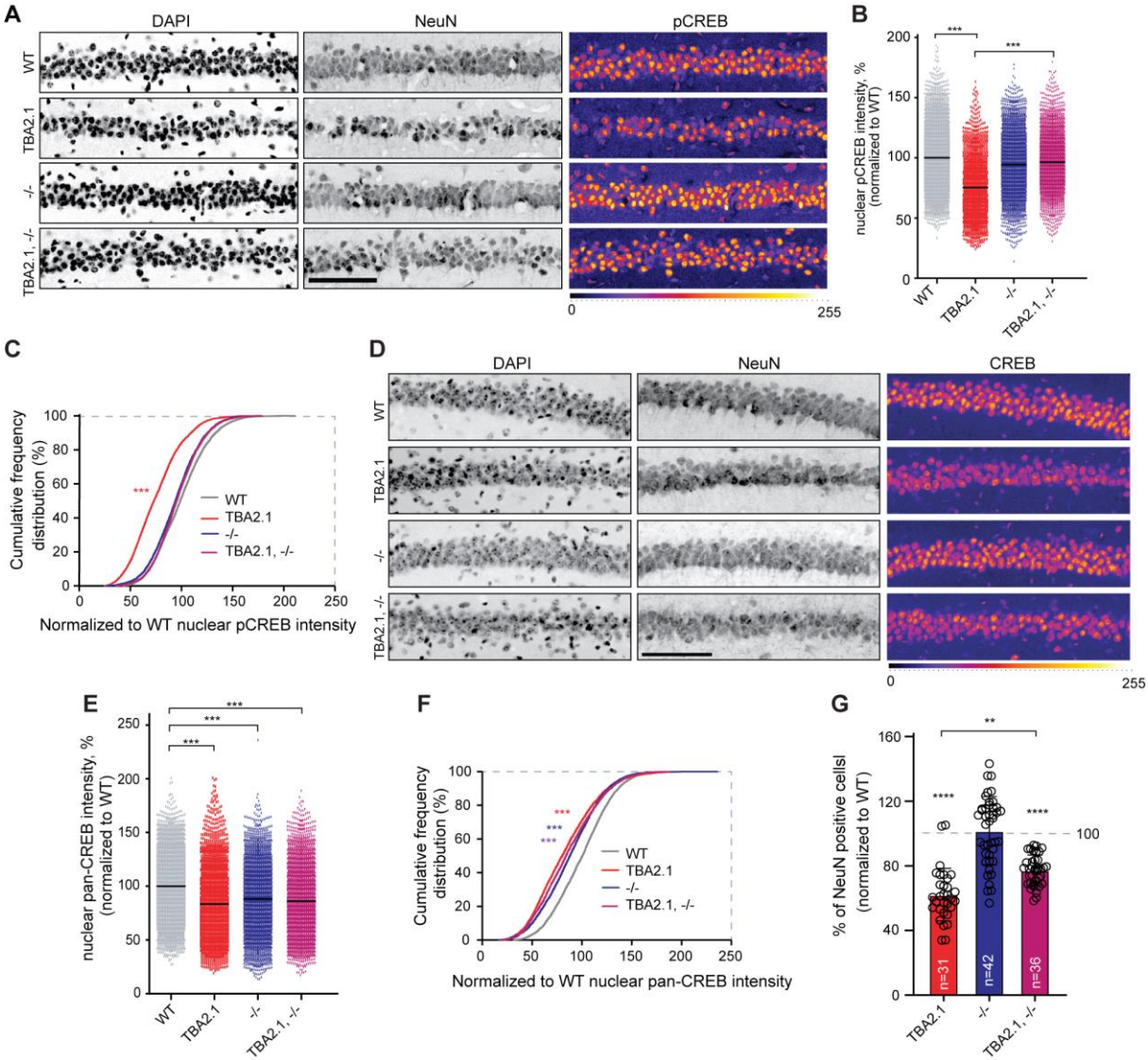

Figure 8. Absence of Jacob rescues the CREB function and neuronal loss in an animal model of AD.

A) Representative confocal images of distal CA1 cryosections from 12 weeks old mice stained for NeuN, DAPI and pCREB. Lookup table indicates the pixel intensities from 0 to 255. Scale bar: 100 µm.

B, C) The quantification of pCREB intensity in NeuN-positive cells revealed a statistically significant decrease in pCREB immunoreactivity in TBA2.1 but not in double transgenic animals (TBA2.1, -/-). Data are represented as (B) dot plot and (C) cumulative frequency distribution. N=655-1232 nuclei from 7-9 animals. ***p<0,001 by two-way ANOVA followed by Bonferroni's multiple comparisons test. Data are represented as mean ± SEM.

D) Confocal images were averaged from two sections of the nuclear layer of distal CA1 stained for NeuN, DAPI and CREB. Scale bar: 100 µm.

E, F) The quantification of CREB intensity in NeuN positive cells revealed a statistically significant decrease in CREB immunoreactivity in Jacob/*Nsmf* knock-out (-/-) and TBA2.1 Jacob/*Nsmf* knock-out (TBA2.1, -/-) mice. Data are represented as (E) dot plot and (F) cumulative frequency distribution of CREB nuclear staining intensity. N=1668-3073 nuclei from 7-9 animals (F). ***p<0,001 by two-way ANOVA followed by Bonferroni's multiple comparisons test.

G) Both TBA2.1 and TBA2.1 Jacob/*Nsmf* knock-out animals (TBA2.1, -/-) display neuronal loss in CA1 region of hippocampus. Bar plot representing the number of NeuN positive cells normalized to WT group. The TBA2.1 Jacob/*Nsmf* knock-out (TBA2.1, -/-) mice display significantly lower degree of neuronal loss compared to TBA2.1 mice. N=31-42 CA1 images analyzed from 9-11 animals per genotype. ****p<0,0001, **p<0,01 by two-way ANOVA followed by Bonferroni's multiple comparisons test. Data are represented as mean ± SEM.

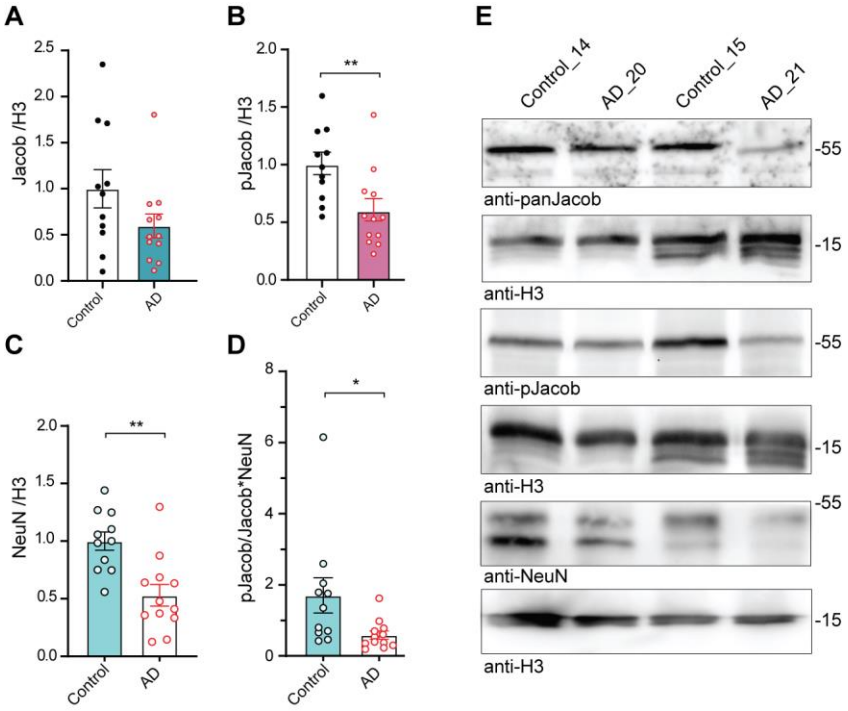

Figure 9. AD patients display decreased amount of pJacob in neurons.

A-D) pJacob, NeuN, as well as pJacob/panJacob ratio by NeuN is decreased in brain samples from AD patients as compared to the control group. Quantification of Jacob (A), pJacob (B), NeuN (C), and pJacob/Jacob ratio (D) by NeuN normalized to Histone3 (H3). N=11-12 protein extracts from different subjects. *p<0,05, **p<0,01 by two-tailed Student t-test. Data are represented as mean ± SEM.
E) Representative image of the immunoblot probed with antibodies against pJacob, pan-Jacob, NeuN and Histone3 (H3).

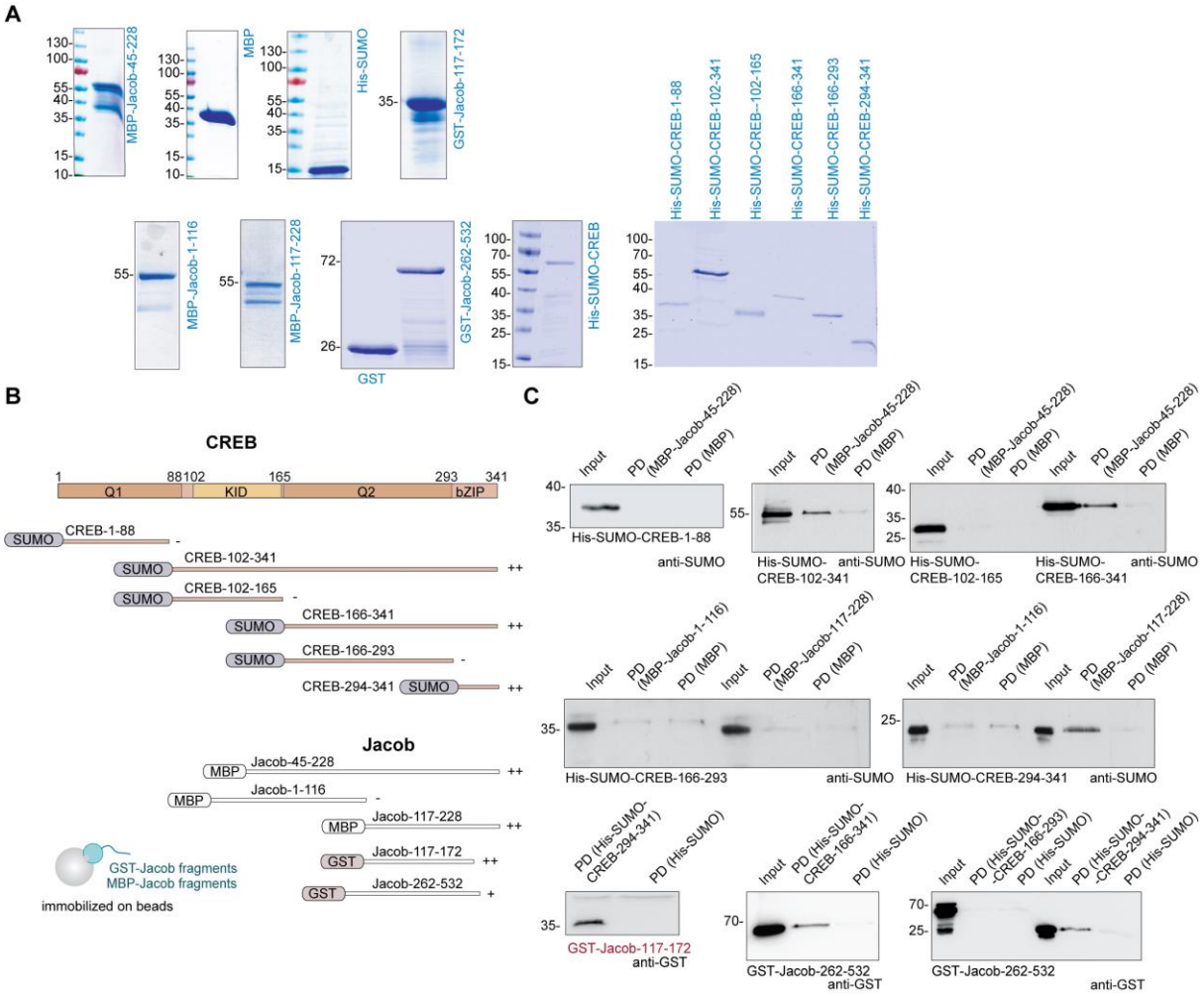

Figure S1 (refers to Figure 1). Mapping of the binding interfaces between Jacob and CREB.

A) Coomassie blue staining depicting the purity of bacterially produced proteins used for pull-down assays between CREB and Jacob.
B) Scheme representing the constructs used for mapping of the interaction sites in Fig. 1D and S1B.
C) The N-terminus of Jacob (117-172 aa in red) interacts with the bZIP domain of CREB, but not with the Q1 (1-88 aa), KID (102-165 aa), or Q2 (166-293 aa) domains. The C-terminus of Jacob (262-532 aa) shows weaker binding to the bZIP domain of CREB. Images of immunoblots representing pull-down assays performed with Jacob and CREB protein fragments depicted in the panel B.

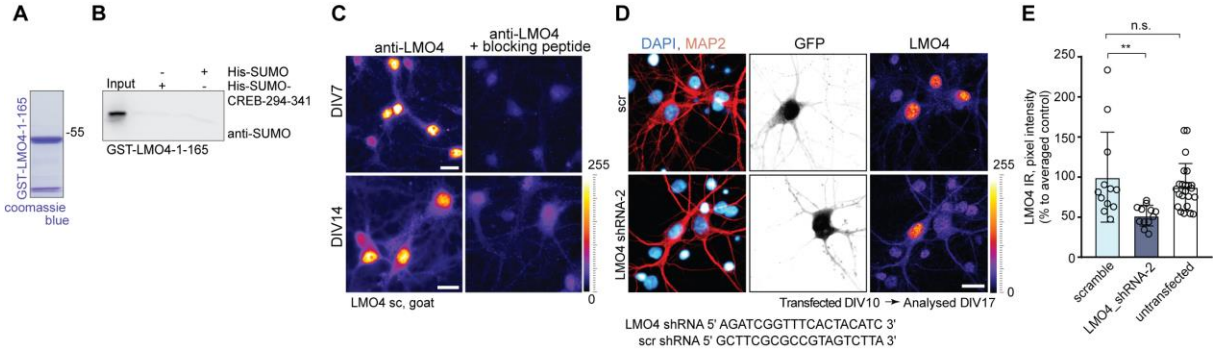

Figure S2 (refers to Figure 2 and 3). Confirmation of LMO4 antibody specificity and quantification of LMO4 knockdown efficiency.

A) Coomassie blue stained gel showing purity of GST-LMO4 used in the pull-down experiments.
B) Pull-down experiments revealed no interaction between His-SUMO-CREB-294-341 with GST-LMO4.
C) A goat C-15 LMO4 antibody (Santa Cruz) was used to stain LMO4 in hippocampal neurons (DIV 7 and DIV 14) in the presence or absence of the blocking peptide. Scale bars: 15 μm.
D) Representative, confocal images of hippocampal neurons transfected with shRNA targeting LMO4 or scrambled control. Reduction of nuclear LMO4 level was confirmed in immunocytochemistry with the goat anti-LMO4 (sc C-15). Scale bar:10 μm.
E) Nuclear LMO4 staining intensity was downregulated in neurons expressing shRNA targeting LMO4 mRNA compared to scrambled-transfected (scr shRNA) or non-transfected cells. Data represented as mean ± SEM. n=12-23 nuclei. **p<0,021 by Kruskal-Wallis test followed by Dunn's multiple comparison test.

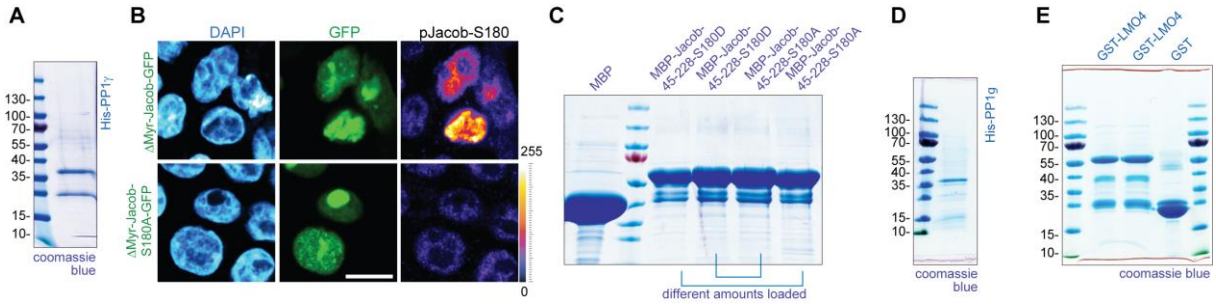

Figure S3 (refers to Figure 6). Protein purity and loading controls for pull down experiments and studies on the interaction depending on Jacob S180 phosphorylation.

A) Coomassie blue stained gel showing purity of commercially available His-PP1γ.
B) Nuclear Jacob (ΔMyr-Jacob-GFP), but not nuclear phosphodeficient mutant (ΔMyr-Jacob-S180A-GFP) expressed in HEK293T cells is phosphorylated. Confocal images of HEK293T cells overexpressing Jacob and immunostained with anti-pS180Jacob antibodies. Scale bar: 10 μm.
C) Images of gels stained with coomassie blue showing the purity of bacterially produced Jacob mutants used for pull-down assay.
E) Images of gels stained with coomassie blue showing the purity of self-purified His-PP1γ.
E) Images of gels stained with coomassie blue showing inputs for bacterially produced GST-LMO4 coupled to beads used for pull-down assay with Jacob and PP1γ.

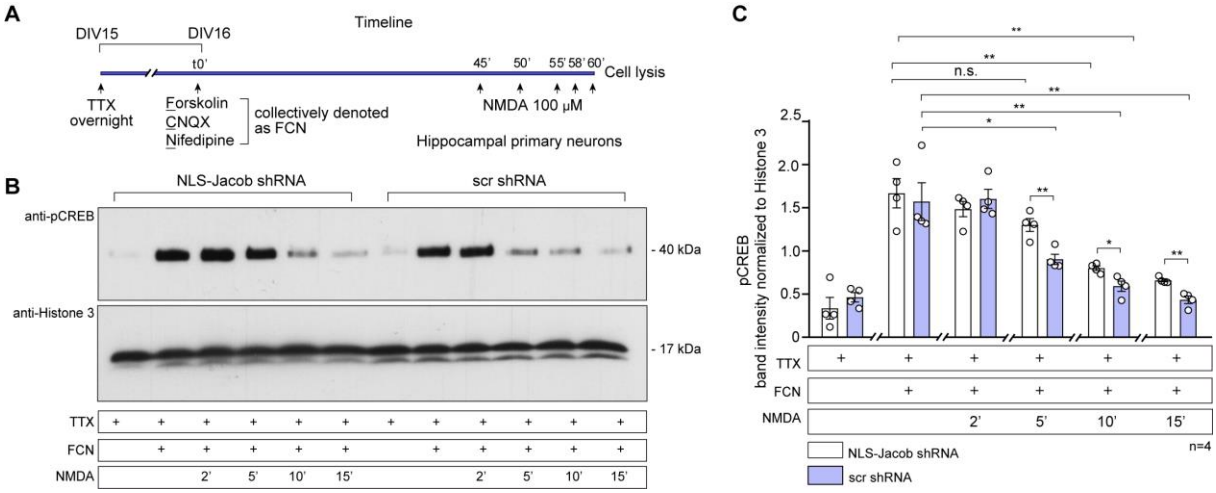

Figure S4. Jacob knockdown partially rescues NMDAR-induced CREB shut-off

A) Scheme representing the timeline of the experiment. Hippocampal cultures were silenced with TTX overnight and subsequently treated with forskolin, CNQX, and nifedipine. The time of NMDA bath application was 2, 5, 10 or 15 minutes.
B) Representative immunoblot of total lysates probed with antibodies detecting pCREB and anti-Histone 3 as a loading control. Hippocampal neurons (DIV6) were infected with lentivirus carrying shRNA-NLS-GFP construct or scrambled control. At DIV15 neurons were treated as depicted in the scheme A.
C) Nuclear Jacob knockdown partially rescues CREB shut-off after 5, 10 and 15 minutes of treatment with NMDA. Bar plot represents quantification of pCREB band intensity normalized to Histone 3. Data are represented as mean ± SEM. n=4 from independent experiments. n.s.- non-significant where p>0,05, *p<0,05, **p<0,01 by two-tailed Student t-test.

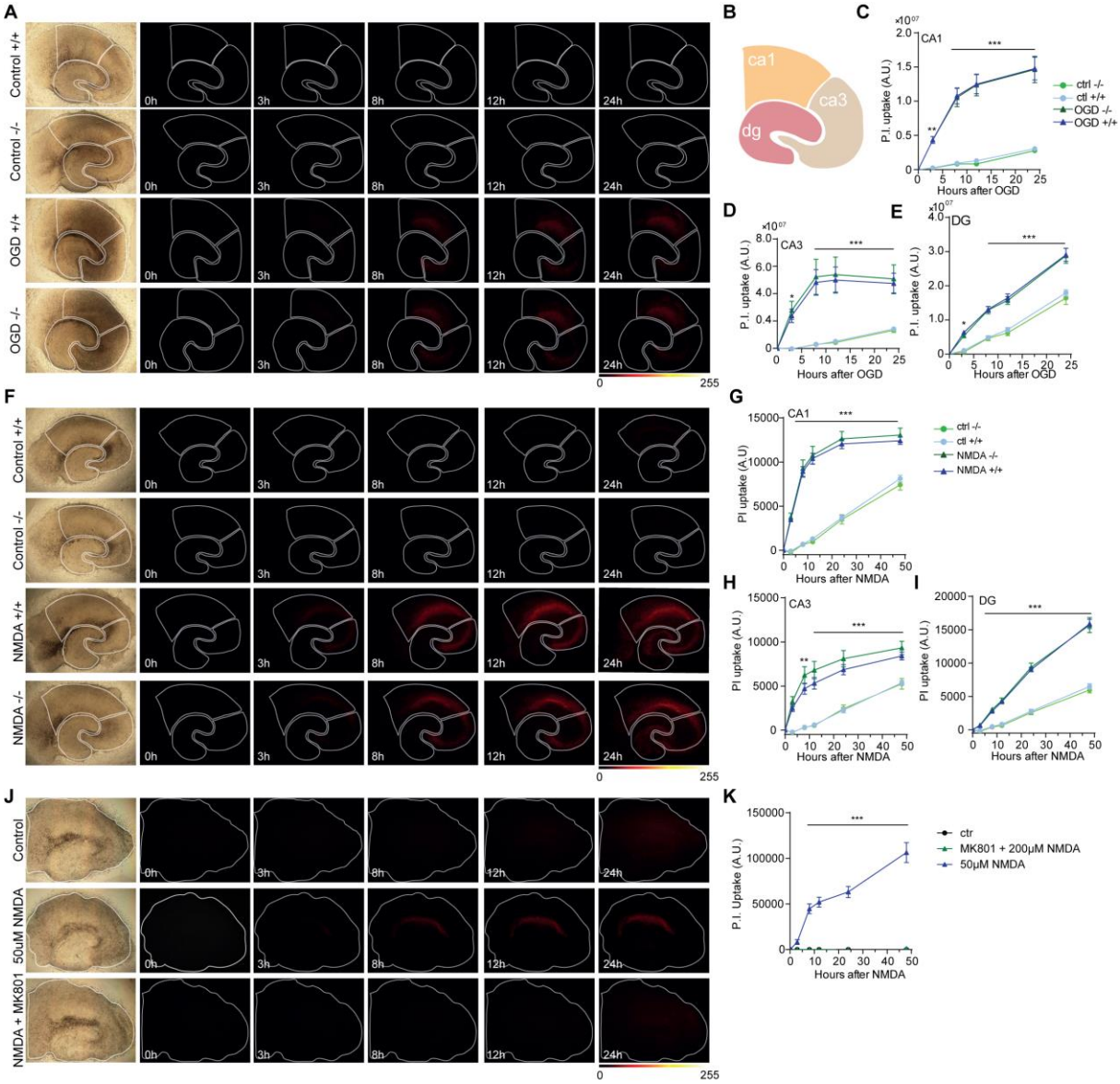

Figure S5. Jacob gene knock-out does not influence the degree of OGD- and NMDA-induced cell death.

A-E) Oxygen glucose deprivation (OGD) induced cell death in organotypic hippocampal slice culture irrespective of mice genotype.

A) Fluorescent images of propidium iodide (PI) signal in organotypic hippocampal slices from wild type (+/+) and Jacob/*Nsmf* constitutive knock-out animals (-/-) after 0, 3, 8, 12, and 24h after 30 min OGD.

B) Scheme representing CA1, CA3, and DG areas.

C-E) Graphs representing the degree of PI uptake (A.U.) over time (h) after OGD insult. The OGD protocol induced cell death to the same degree in CA1(C), CA3 (D), and DG (E) irrespective of genotype. N=7-13 slices per group. **p<0,01, ***p<0,001 vs. control by RM-2way ANOVA followed by Bonferroni's multiple comparisons test. Data represented as mean ± SEM.

F-I) Acute NMDA (50 µM) treatment induces the cell death in organotypic hippocampal slice culture irrespective of genotype.

F) PI signal in organotypic hippocampal slices from wild type (+/+) animals after 0, 3, 8, 12, and 24h post treatment with 50 µM NMDA.

G, H, I) Graphs representing the degree of PI uptake (A.U.) over time (h) after treatment with 50 µM NMDA. The 50 µM NMDA induced cell death to the same degree in CA1, CA3, and DG irrespective of genotype. N=6-15 slices per group. **p<0,01, ***p<0,001 vs. control by repeated measure two-way ANOVA followed by Bonferroni's multiple comparisons test. Data represented as mean ± SEM.
J-K) MK801 blocks NMDA-induced cell death in organotypic slice culture irrespective of mice genotype. (J) PI signal in organotypic hippocampal slices from wild type (+/+) animals after 3, 8, 12, 24, and 48h after treatment with 50 µM NMDA. (K) The co-application of MK-801 completely abolished the effects of NMDA treatment. N=4-8 slices per group. ***p<0,001 vs. control by repeated measure two-way ANOVA followed by Bonferroni's multiple comparisons test. Data represented as mean ± SEM. Lookup table indicates the pixel intensities from 0 to 255.

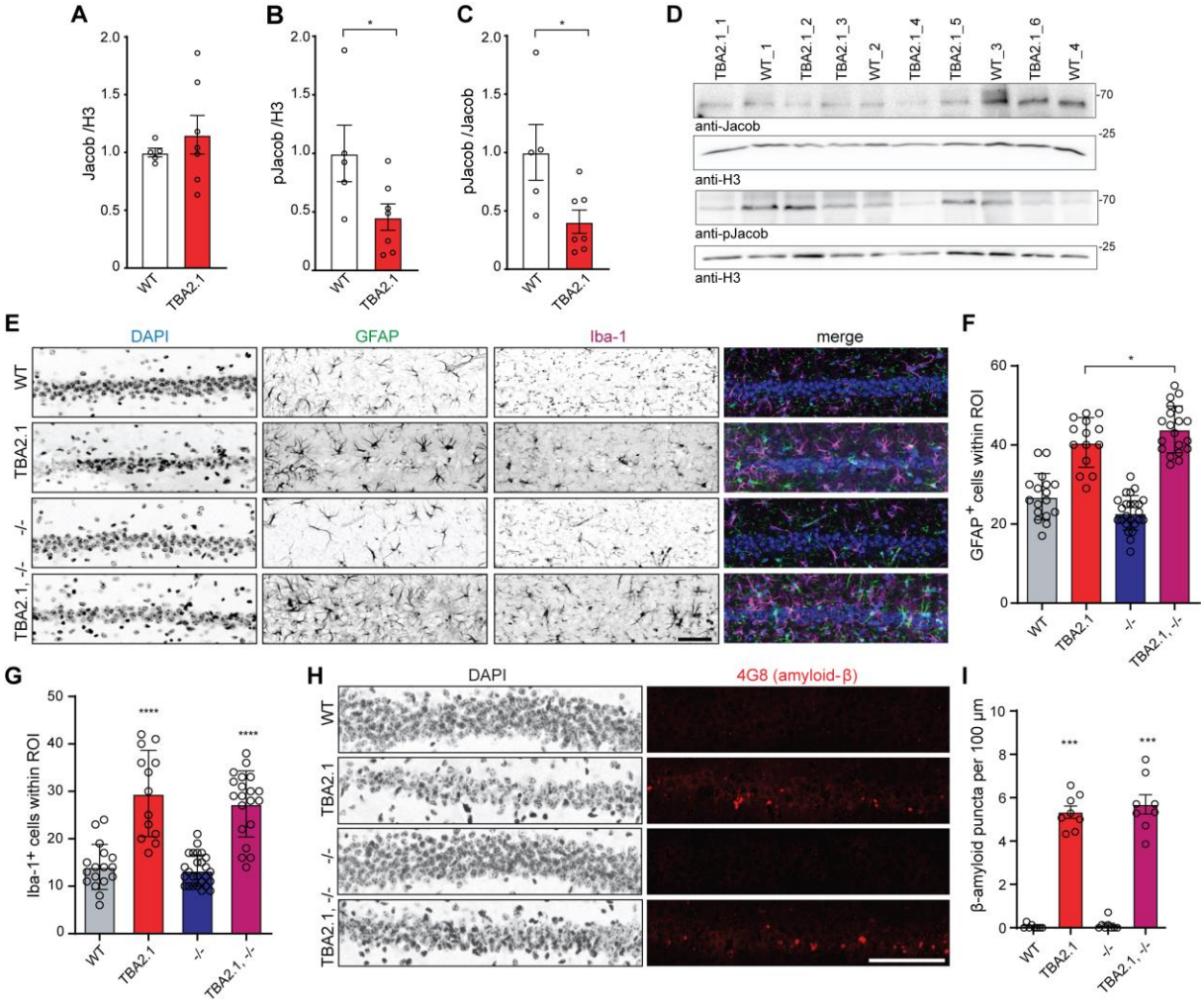

Figure S6. Jacob/Nsmf deletion does not impact increased number of activated microglia, astrocytes and prominent deposition of amyloid-β in plaques.

A-C) pJacob level and pJacob/panJacob ratio are decreased in TBA2.1 mouse line compared to WT animals. Quantification of Jacob level (A), pJacob level (B) and pJacob/Jacob ratio (C) normalized to Histone3 (H3). N=5-7 hippocampal, protein extracts. *p<0,05 by two-tailed Student t-test. Data are represented as mean ± SEM.
D) Representative images of immunoblots probed with antibodies against pJacob (S180), panJacob and Histone3.
E) Representative confocal images of distal CA1 sections from 12 weeks old mice stained for GFAP, DAPI and Iba-1. Scale bar: 100 µm.
F) Bar plot representing the number of GFAP positive cells per rectangular region of interest. N=17-24 cryosections from 5-7 animals per genotype. ****p<0,0001, *p<0,05 by two-way ANOVA with Bonferroni post hoc test. Data are represented as mean ± SEM.
G) Bar plot representing the number of Iba-1 positive cells per rectangular region of interest. N=17-26 cryosections from 5-7 animals per genotype. ****p<0,0001 by two-way ANOVA with Bonferroni post hoc test. Data are represented as mean ± SEM.
H) Confocal images averaged from two sections of the molecular layer of 12 weeks old mice distal CA1 labelled for amyloid-β (4G8 antibody) and co-stained with DAPI. Scale bar: 100 µm.

I) Bar plot representing the number of amyloid-β positive puncta per 100 µm. N=8, number of cryosections from 2 animals per genotype. ***p<0,001 by two-way ANOVA with Bonferroni post hoc test. Data are represented as mean ± SEM.

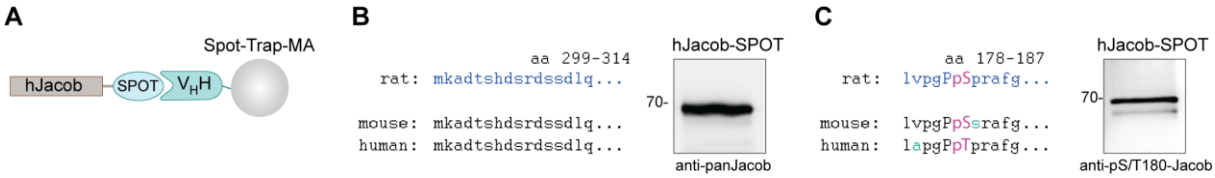

Figure S7. Anti-panJacob and anti-pJacob antibodies generated against rat peptide detect the human protein.

A) Schematic represents the immunoprecipitation approach employing Spot-nano Trap coupled to magnetic agarose (Chromotek) used for the enrichment of hJacob expressed in HEK293T cells for antibody detection.
B) Rat amino acid sequence of Jacob used for generation of pan-Jacob antibodies is conserved throughout the species and the antibody effectively detects human Jacob.
C) Despite variability within the peptide amino acid sequence used for the production of polyclonal pJacob antibodies they do recognize the human protein.

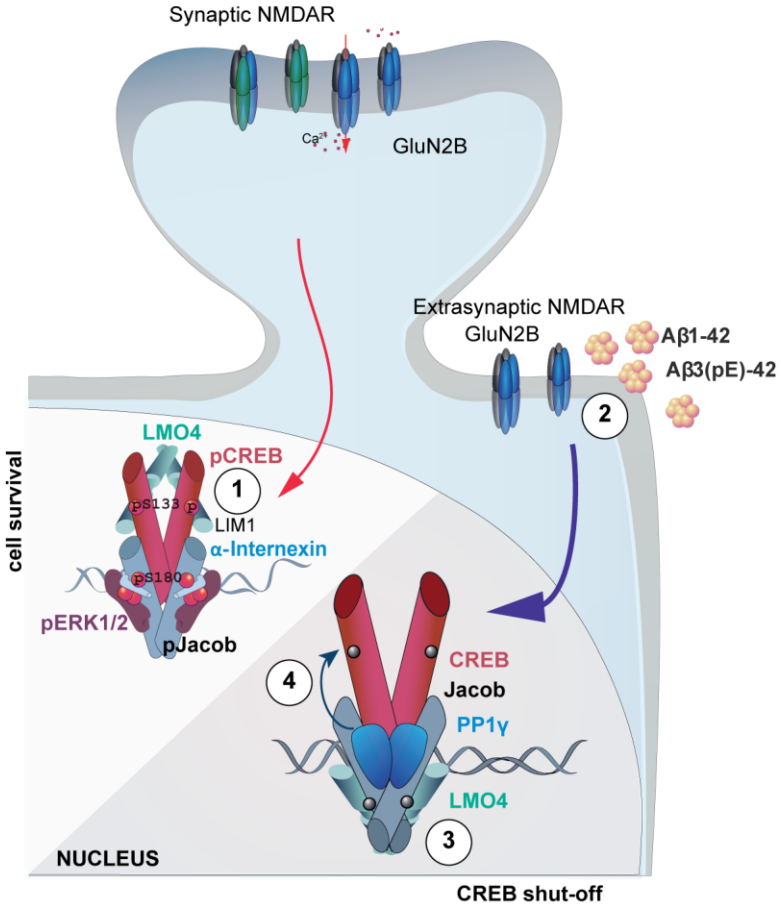

Figure S8. Summary

A) Jacob docks a signalosome to CREB that encodes the synaptic (1) or extrasynaptic (2) origin of the NMDAR signal. Following synaptic NMDAR activity Jacob docks the MAP-kinase ERK to CREB which results in sustained CREB activation (1). In case of disease-related stimulation of extrasynaptic NMDAR with amyloid-β dephosphorylated Jacob associates with the CREB adaptor protein LMO4 and replaces it from the CREB complex (3). In parallel, the association with LMO4 enhances binding of Jacob to PP1γ and this complex induces long-lasting dephosphorylation and transcriptional inactivation of CREB in the context of early synaptic dysfunction and cell loss in AD (4).

Supplementary Table 1. Summary of cases used in the study and PM delay of tissue collection for each case.

Number	Gender	Age	PM delay, hrs	Group
1	m	93	93	AD
2	w	74	74	Control
3	w	86	86	AD
4	m	67	67	Control
6	m	50	50	Control
7	m	52	52	Control
8	m	76	76	AD
9	m	65	65	Control
10	w	83	83	AD
11	w	81	81	AD
12	w	77	77	AD
13	w	84	84	Control
14	m	82	82	Control
15	m	44	44	Control
16	w	53	53	Control
17	w	72	72	Control
18	w	84	84	Control
19	m	69	69	AD
20	m	73	73	AD
21	w	64	64	AD
22	w	88	88	AD
23	w	82	82	AD
24	m	80	80	AD

Supplementary Table 2. Description of the antibodies, constructs and oligonucleotides used in this study and corresponding sources.

REAGENT or RESOURCE	SOURCE	IDENTIFIER	Application
Recombinant DNA			
I. Jacob cDNA / constructs *(rat sequence if not specified)*			
Jacob-1-228	(28); pGBKT7	N/A	YTH-System
Jacob-1-228	(28); pGADT7	N/A	YTH-System
Jacob-262-532	This paper, pGBKT7	N/A	YTH-System
Jacob-1-116	This paper, pGBKT7	N/A	YTH-System
Jacob-117-228	This paper, pGBKT7	N/A	YTH-System
Jacob-167-193	This paper, pGBKT7	N/A	YTH-System
Jacob-175-201	This paper, pGBKT7	N/A	YTH-System
Jacob-202-228	This paper, pGBKT7	N/A	YTH-System
Jacob -117-228	This paper, pGAD-T7	N/A	YTH-System
Jacob -167-193	This paper, pGAD-T7	N/A	YTH-System
Jacob -175-201	This paper, pGAD-T7	N/A	YTH-System
Jacob -202-228	This paper, pGAD-T7	N/A	YTH-System
Jacob -202-228	This paper, pGAD-T7	N/A	YTH-System
Jacob-GFP	(27); pEGFP-N1 (Clontech)	N/A Cat.: #6085-1	Heterologous Co-IP, WB, FRET assay
Jacob-SPOT (human sequence)	This paper, pRP(Exp)-CMV (VectorBuilder)	N/A	IP with SPOT-Trap_MA, (Chromotek)
Jacob-tRFP	This paper, tagRFP-N1 (vector backbone Clontech, eGFP exchanged with tagRFP Evrogen)	N/A	Heterologous Co-IP, WB
ΔMyr-Jacob-GFP	(27)	N/A	FRET assay, Co-recruitment assay

ΔMyr-Jacob-S180A-GFP	(27)		ICC
ΔMyr-Jacob-Myc	(28)	N/A	CREB co-activation assay
ΔMyr-Jacob-S180A-Myc	(28)	N/A	CREB co-activation assay
Jacob-1-228-GFP	This paper, pEGFP-N1	N/A	FRET assay, Co-recruitment assay
Jacob-262-532-GFP	This paper, pEGFP-N1	N/A	FRET assay
Jacob-L175A-V176A-GFP	This paper, pEGFP-N1	N/A	Heterologous Co-IP
Jacob-1-246-GFP	This paper, pEGFP-N1	N/A	Heterologous Co-IP
Jacob-247-532-GFP	This paper, pEGFP-N1	N/A	Heterologous Co-IP
Jacob-1-172-GFP	This paper, pEGFP-N1	N/A	Heterologous Co-IP
Jacob-173-246-GFP	This paper, pEGFP-N1	N/A	Heterologous Co-IP
Jacob-247-309-GFP	This paper, pEGFP-N1	N/A	Heterologous Co-IP
Jacob-310-532-GFP	This paper, pEGFP-N1	N/A	Heterologous Co-IP
Jacob-213-246-GFP	This paper, pEGFP-N1	N/A	Heterologous Co-IP
Jacob-173-246-GFP	This paper, pEGFP-N1	N/A	Heterologous Co-IP
MBP-Jacob-45-228	This paper, pMAL-c5x, (NEB)	N/A Cat.: #P8010	PD assay
MBP-Jacob-1-116	This paper, pMAL-c5x	N/A	PD assay
MBP-Jacob-117-228	This paper, pMAL-c5x	N/A	PD assay
MBP-Jacob-262-532	This paper, pMAL-c5x	N/A	PD assay
GST-Jacob-262-532	This paper, pGEX-5X-1 (Sigma-Aldrich	N/A Cat: #GE28-9545-53	PD assay
MBP-Jacob-45-228	This paper, pMAL-c5x, (NEB)	N/A	PD assay
MBP-Jacob-45-228-S180D	This paper, pMAL-c5x, (NEB)	N/A	PD assay
MBP-Jacob-45-228-S180A	This paper, pMAL-c5x, (NEB)	N/A	PD assay
Jacob shRNA 5′AGAATGATTCCGCGTCTGTAA 3′	(27)	N/A	ICC

Jacob scr shRNA 5′AGATATAGTCGCCGTC TG TAA 3′	(27)	N/A	ICC
II. LMO4 cDNA / constructs *(mouse, rat and human sequences are identical)*			
LMO4	This paper, pACT2	N/A	YTH-System
LMO4	This paper, pGBKT7	N/A	YTH-System
LIM1-1-80	This paper, pGAD-T7	N/A	YTH-System
LIM2-81-165	This paper, pGAD-T7	N/A	YTH-System
LMO4-tagRFP	This paper, tagRFP-N1	N/A	Heterologous Co-IP, Co-recruitment assay
LIM1-1-80-tagRFP	This paper, tagRFP-N1	N/A	Co-recruitment assay, FRET assay
LIM2-81-165-tagRFP	This paper, tagRFP-N1	N/A	Co-recruitment assay, FRET assay
GST-LMO4	This paper, pGEX-5X-1, (Sigma-Aldrich)	N/A Cat.:#GE28-9545-53	PD assay
LMO4-GFP	This paper, pEGFP-N3 (Clontech)	N/A Cat.:#6080-1	FRET assay
Myc-LMO4	This paper, pcDNA	N/A	CREB co-activation assay
shRNA targeting sequence: LMO4 5´-AGATCGGTTTCACTACA TC -3´	psiHIV-H1, (GeneCopoeia)	N/A	-
LMO4_shRNA 5´-AGATCGGTTTCACTACA TC -3´	FUGW-H1w	N/A	ICC
LMO4_scrambled shRNA 5´-GCTTCGCGCCGTAGTCT TA-3´	FUGW-H1w	N/A	ICC
III. CREB cDNA / constructs *(human sequence)*			
CREB-tagRFP	This paper, tagRFP-N1	N/A	Heterologous Co-IP
CREB-GFP	This paper, pEGFP-N1	N/A	FRET assay

CREB-Rluc	This paper, pRLuc-N1 vector (pRLuc-N1 PerkinElmer)	Cat.:#TDS-6310200; discontinued	SRET assay
CREB-1-165-tagRFP	This paper, tagRFP-N1	N/A	FRET assay
CREB-166-341-tagRFP	This paper, tagRFP-N1	N/A	FRET assay
His-SUMO-CREB	This paper, pET-6xHis-SUMO	N/A	PD assay
His-SUMO-CREB-1-88	This paper, pET-6xHis-SUMO	N/A	PD assay
His-SUMO-CREB-1-165	This paper, pET-6xHis-SUMO	N/A	PD assay
His-SUMO-CREB-1-293	This paper, pET-6xHis-SUMO	N/A	PD assay
His-SUMO-CREB-89-314	This paper, pET-6xHis-SUMO	N/A	PD assay
His-SUMO-CREB-89-165	This paper, pET-6xHis-SUMO	N/A	PD assay
His-SUMO-CREB-166-341	This paper, pET-6xHis-SUMO	N/A	PD assay
His-SUMO-CREB-166-293	This paper, pET-6xHis-SUMO	N/A	PD assay
His-SUMO-CREB-294-341	This paper, pET-6xHis-SUMO	N/A	PD assay
IV. Other constructs			
NLS-GFP	This paper	N/A	ICC
CDD-GFP (Caldendrin)	(27)	N/A	FRET assay
Champion™ pET-6xHis-SUMO	Termo Fisher Scientific	Cat.: #K30001	PD assay
tagRFP	Evrogen	Cat.: #FP142	Heterologous Co-IP
GFP-PP1 gamma, (human sequence)	Addgene, (85)	Cat.: #44225	Heterologous Co-IP
mCherry-PP1 gamma, (human sequence)	Addgene, (86)	Cat.: #45220	Heterologous Co-IP
pGL4.29[luc2P/CRE/Hygro] Vector	Promega	Vector Cat.: #E847A	Reporter assay
His-PP1 gamma, (human sequence)	pET28	N/A	PD assay
Recombinant Human PP1 gamma (PPP1CC), His-tag	Creative BioMart	(Cat. PPP1CC-84, Lot no. 201811)	PD assay
Antibodies and peptides	**SOURCE**	**IDENTIFIER**	**Application/ Dilution**

Blocking peptide for anti-LMO4 antibodies, against human C-terminus	Santa Cruz	(C-15) Sc-11122p	ICC
anti-Jacob-87, rabbit polyclonal (against EQPPLPEASGRHKKLER rat Jacob peptide – 187-203 aa)	(83)	Cat.: # N/A RRID: N/A	WB/ ICC/STED 1:1000/1: 300/1:100
anti-MBP, mouse monoclonal	NEB	Cat.: # E8032L RRID: AB_1559730	WB 1:5000
anti-SUMO, rabbit polyclonal	This paper	Cat.: # N/A RRID: N/A	WB 1:2000
anti-Jacob 1384, rabbit polyclonal (against MKADTSHDSRDSSDLQ rat Jacob peptide – 299-314 aa)	(28) custom made	Cat.: # N/A RRID: N/A	WB 1:1000
anti-pJacob Ser180, rabbit polyclonal (against synthetic phosphorylated peptide LVPGpSPRAFG - 178-187 aa)	(28) custom made, BioGenes	Cat.: # N/A RRID: N/A	WB 1:750
anti-CREB, 48H2, rabbit monoclonal	Cell Signaling Technology	Cat.: #9197, RRID: AB_331277	ICC/ICH 1:300
anti-CREB, D76D11, rabbit monoclonal	Cell Signaling Technology	Cat.: #4820 RRID: AB_1903940	WB 1:1000
anti-CREB LB9, mouse monoclonal	Thermo Fisher Scientific	Cat.: #MA1-083 RRID: AB_558523	ICC/STED 1:150
anti-pCREB (Ser133), rabbit polyclonal	Millipore	Cat.: #06-519, RRID: AB_310153	IHC/WB 1:400/1:1000
Anti-PP1 gamma; rabbit polyclonal	Thermo Fisher scientific	Cat.: #PA5-21671 RRID: AB_11153939	WB 1:500
anti-MAP2, mouse monoclonal	Sigma-Aldrich	Cat.: # M-4403; RRID: AB_477193	ICC/ICH 1:1000/1:500
NeuN, mouse monoclonal 1:400	Millipore	Cat.: #MAB377; RRID: AB_2298772	IHC 1:400

LMO4, goat polyclonal	Santa Cruz	Cat.: #sc-11122, RRID: AB_648429	ICC/ STED 1:300/1:100
GFAP, rabbit polyclonal	Sigma-Aldrich	Cat.: #G-9269; RRID: AB_477035	IHC 1:400
Iba-1, guinea pig	SySy	Cat.: #234004; RRID: AB_2493179	ICH: 1:400
Amyloid β (clone 4G8), mouse monoclonal	BioLegend	Cat.: #800701 RRID: AB_2564633	IHC
anti-histone 3 (H3), rabbit monoclonal	NEB	Cat.: #4499; RRID: AB_10544537	WB 1:1000
anti-GFP (B34); mouse monoclonal	BioLegend	Cat.: # 902601 RRID: AB_2565021	Heterologous Co-IP, WB 1:1000
anti-tagRFP; rabbit polyclonal	Evrogen	Cat.: #AB233; RRID: AB_2571743	Heterologous Co-IP, WB 1:1000
anti-RFP, rabbit polyclonal	Rockland	Cat.: #600-401-379, RRID: AB_2209751	Heterologous Co-IP, WB 1:1000
Anti-rabbit-AlexaFluor 488	ThermoFisher Scientific	Cat.: #A-11034; RRID: AB_2576217	ICC/IHC 1:500
Anti-rabbit-AlexaFluor 568	ThermoFisher Scientific	Cat.: #A-11036; RRID: AB_10563566	ICC/IHC 1:500
Anti-mouse-AlexaFluor 488	ThermoFisher Scientific	Cat.: #A-11001; RRID: AB_2534069	ICC/IHC 1:500
Anti-mouse-AlexaFluor 568	ThermoFisher Scientific	Cat.: #A-11004; RRID: AB_2534072	ICC/IHC 1:500
Anti-guinea pig-AlexaFluor 647	ThermoFisher Scientific	Cat.: #A-21450; RRID: AB_2535867	ICC/IHC 1:500
Anti-rabbit-IgG-HRP	Dianova	Cat.: #111-035-114 RRID: AB_2337938	WB 1:10000
Anti-mouse-IgG-HRP	Dianova	Cat.: #115-035-146 RRID: AB_2307392	WB 1:10000

Anti-guinea pig-IgG-HRP	Dianova	Cat.: #705-035-147; RRID: AB_2337022	WB 1:10000
anti-goat AlexaFluor 568	Thermo Fisher Scientific	Cat.: # A-11057 RRID: AB_2534104	ICC/STED 1:200
anti-rabbit Abberior STAR 635P	Abberior	Cat.: #2-0012-007-2	ICC/STED 1:250
anti-mouse Abberior STAR 635P	Abberior	Cat.: # 2-0002-007-5	ICC/STED 1:250
anti-rabbit Abberior STAR 580	Abberior	Cat.: # 2-0012-005-8	ICC/STED 1:250